DTU Physics
Department of Physics

C:O:N:T
Copenhagen Graduate School in
Nanoscience and Nanotechnology

CAMd
Center for Atomic-scale Materials Design

PROJECTOR AUGMENTED WAVE CALCULATIONS WITH LOCALIZED ATOMIC ORBITALS

MASTER THESIS

Marco Vanin

s060662

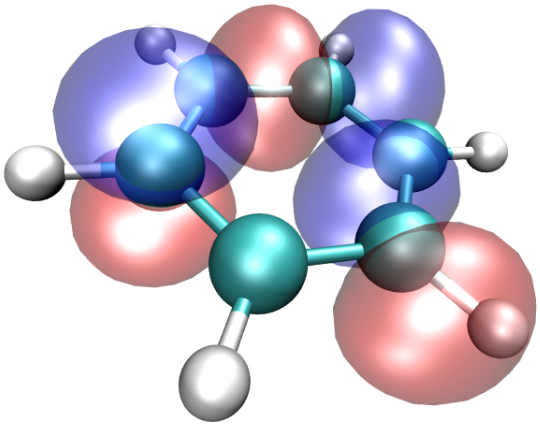

Center for Atomic-Scale Materials Design
Department of Physics
Technical University of Denmark

Cover illustration: a benzene molecule and three basis orbitals for carbon, namely p_x, p_y and p_z, located at every second carbon atom.

Preface

This thesis is submitted in candidacy for the Master of Science degree at the Technical University of Denmark, within the field of Physics and Nanotechnology. The work has been carried out from September 2007 to June 2008 at the Center for Atomic-scale Materials Design (CAMD), Department of Physics, DTU, with Kristian Thygesen and Jens Jørgen Mortensen as supervisors. Financial support was provided by the Copenhagen Graduate School for Nanoscience and Nanotechnology (CONT).

I would like to thank the institution and the individuals that made it possible for me to handle this challenge. Most of the work has been done in collaboration with Ask Hjorth Larsen, to whom I am grateful for a very fruitful collaboration. I am grateful to Kristian Thygesen for the guidance and for the many helpful and stimulating wide-ranging discussions. I sincerely thank Jens Jørgen Mortensen for infinite support and help, especially with the GPAW code and related issues. Actually, a great part of the challenge in this project has been the computational aspect, which was not a major part of my background. The parallel study of theoretical methods and in particular DFT has also been a significant part of the work, helped by the stimulating environment provided by CAMD and, of course, by the essential coffee. I would also like to thank professor Karsten Wedel Jacobsen for his enthusiasm and suggestions provided during our "Tuesday meetings".

Thanks to Mikkel Strange for providing me with the electron transport test-calculation presented in section 6.4. and to Carsten Rostgaard for proofreading and "gym-breaks".

Of course, thanks to my family for distant but ever-present love and support, and a special thanks to Silvia for near love and support as well as for providing me with pleasant distractions from physics, math and computations.

Copenhagen, June 2008

Marco Vanin

Abstract

This thesis concerns theoretical-computational work within the framework of Density Functional Theory. A localized basis set is included in the Projector Augmented Wave formalism and implemented in its real-space grid-based version GPAW. This enables fast and efficient calculations done with the same approximations of the grid-based implementation. The complementarity of the two schemes can then be combined in a very flexible way, driven by the specific application. The presented benchmark calculations show an overall good accuracy with respect to the grid results.

Contents

Chapter 1

Introduction

In the early 1930s physicists were formally aware of the quantum theory, that is to say they had the set of equations governing systems of many electrons. Together with chemists, they developed several methods and approximations, but it was only the Density Functional Theory (DFT) [15] [22], pioneered by W. Kohn, P. Hohenberg and L. Sham, which paved the way for accurate quantum mechanical calculations at a reasonable computational cost. Inspired by basics ideas of solid state physics, it is a formally exact quantum theory that has become the method of choice for calculations on realistic systems. In recent years it has also become popular in the quantum chemistry community, due to the improvement in the accuracy of its approximated functionals.

Thanks also to the enormous increase in computer power, density functional calculations are now becoming feasible on large scale systems. This new computational capability opens up great perspective in many fields and disciplines where atomic-scale understanding would be relevant. Large biomolecules, nano-materials and devices, complex chemical reactions are few examples.

Many different implementations of the theory are today available in the literature. Most notably the Projector Augmented Wave (PAW) method [5] is an efficient generalization of both the pseudopotential and the augmented waves methods providing an elegant framework for large calculations with all-electron quality.

The aim of this work is to enable density functional calculations by means of efficient local basis sets at the level of the PAW theory. The PAW method was already implemented in a real-space grid version in the GPAW code [17] [1]. The PAW method itself is already very efficient compared to traditional all-electron approaches. The combination with a local basis set is then promising for treating complex systems of many electrons still preserving all-electron accuracy. A unique feature of this work is that the possibility to carry out basis-set calculations shares the exact same approximations of the

full-grid counterpart. This provides a great flexibility, allowing to switch between basis-set and grid representation of the wavefunction thus exploiting the complementarity of the two schemes. For instance the grid provides the natural complete basis set limit, and thus very accurate calculations while a minimal basis-set could be used to obtain good initial guesses as well as fast results. For instance one could efficiently relax complex structures, and then switch to the grid for possible last iterations in the minimization procedure. Furthermore, the localized basis is well suited for quantum transport calculations, linear-scaling computation schemes, molecular dynamics simulations, as well as for analysis purposes.

In this work, the derivation of the equations needed to handle a basis set in the PAW formalism has been carried out. The implementation has been done in the GPAW code and some benchmark results are presented.

Outline of the thesis

The remainder of this thesis is organized as follows:

Chapter 2 provides a brief theoretical background in Density Functional Theory (DFT).

Chapter 3 introduces the Projector Augmented Wave (PAW) formalism, which is the theoretical framework of this work.

Chapter 4 addresses some general issues related to different ways of implementing the theory.

Chapter 5 presents how a localized basis is included in the PAW formalism. This contains the changes that were needed in the real space code in order to handle a finite basis.

Chapter 6 contains and discusses numerical results. This is done through tests and benchmark calculations on several physical systems.

Units

Atomic units are used throughout this thesis. In this units the length unit is the Bohr radius a_0, the charge unit is the electron charge e and the mass unit is the mass of the electron m_e, i.e. $m_e = e = \hbar = a_0 = 1$.

Chapter 2

The Many-Body Problem

Atoms, molecules, clusters and condensed matter systems consist of mutually interacting electrons and nuclei. The behavior of such a quantum system is then described by a Hamiltonian operator which depends on both the electronic and ionic degrees of freedom. In coordinate representation this means that the wave function depends on both the nuclear and electronic spatial coordinates.

The first major simplification is brought by the Born-Oppenheimer approximation, which allows to decouple the electronic and ionic part because of the large difference in mass between the electrons m_e and the ions M_I, $10^{-3} \leq m_e/M_I \leq -10^{-5}$. The electron problem can thus be reduced to a N-electron Hamiltonian in which the nuclei are assumed to be fixed at some given positions $\{\mathbf{R}_I\}$, i.e. they enter as external parameters. In the non-relativistic approximation it reads

$$\begin{aligned} \hat{H} &= -\frac{1}{2}\sum_{i=1}^{N}\nabla_i^2 - \sum_i\sum_I \frac{Z_I}{|\mathbf{r}_i - \mathbf{R_I}|} - \sum_{i<j}^{N}\frac{1}{|\mathbf{r}_i - \mathbf{r_j}|} \\ &= \hat{T} + \hat{V}_{ext} + \hat{V}_{e-e} \end{aligned} \tag{2.1}$$

where $\mathbf{r}_i$ is the position of electron i and Z_I is the atomic number of nucleus I. The first term in (2.1) is the kinetic energy operator, the second term is the electrostatic potential from the ions and the last term is the electron-electron interaction due to the Coulomb repulsion between electrons. We note that $\hat{V}_{ext}$ could also include any other external contribution (e.g. applied electromagnetic fields) besides the ionic potential. The electronic many-body wave function must then obey the Schrödinger equation

$$\hat{H}\Psi(\mathbf{r_1}\sigma_1, \mathbf{r_2}\sigma_2, ..., \mathbf{r_N}\sigma_N,) = E\Psi(\mathbf{r_1}\sigma_1, \mathbf{r_2}\sigma_2, ..., \mathbf{r_N}\sigma_N,) \tag{2.2}$$

where σ_i is the spin variable for electron i. It should be noted that all the many-body effects are contained in the two-body operator $\hat{V}_{e-e}$, which is then the most cumbersome term to deal with in realistic calculations.

Solving (2.2) is the fundamental issue in the theory of the electronic structure of matter, and many ways of attacking the problem have been developed, based on different approximations. For sufficiently small molecules, wavefunction-based methods are feasible and give excellent results. They usually rely on the minimization of a suitable energy functional within the space of a chosen set of approximations for the real wave-function. Many-body perturbation theory is another approach, but extremely expensive numerical methods are required for realistic systems. Quantum Monte Carlo simulations are also computationally very demanding, restricting them only to systems with a few electrons.

A somewhat different approach is provided by the Density Functional Theory (DFT), which has became the basis of much of the computational many-body physics we see today.

2.1 Density Functional Theory

> The fundamental laws necessary for the mathematical treatment of a large part of physics and the whole of chemistry are thus completely known, and the difficulty lies only in the fact that application of these laws leads to equations that are too complex to be solved.

This is from P.A.M Dirac, after the Schrödinger equation had been written and applied to the simplest possible systems. Although much progress has been made in finding approximate solutions, Dirac's point is practically still valid today if we consider solving directly the Schrödinger equation. This is where the Density Functional Theory comes in as an alternative approach to the theory of electronic structure where the electron density $n(\mathbf{r})$, rather than the many-body wave function $\Psi(\mathbf{r_1}\sigma_1, \mathbf{r_2}\sigma_2, ..., \mathbf{r_N}\sigma_N)$, plays the main role [21]. This is remarkably important both numerically and from a conceptual point of view, since it represents an exact ground-state quantum theory equivalent to the Schrödinger approach. For the pioneering work in this field Walter Kohn was indeed awarded the Nobel Prize in Chemistry in 1998, shared with John Pople.

Nevertheless, although in principle exact, the theory requires a universal functional[1] $F[n(\mathbf{r})]$ which is in general unknown and must then be approximated.

2.1.1 Hohenberg-Kohn theorems

The formal starting point is the work by Hohenberg and Kohn (HK) in 1964 [15]

[1] i.e. which applies to *all* electronic systems in their ground state, no matter what the external potential is.

Theorem 2.1.1 (Hohenberg-Kohn 1,1964) *The ground state density* $n(\mathbf{r})$ *of a many-body quantum system in some external potential* $v_{ext}(\mathbf{r})$ *determines this potential uniquely.*

which formally enables using the three-dimensional (real) function $n(\mathbf{r})$ instead of the 3N-dimensional (complex) many-body wave function $\Psi(\mathbf{r_1}, \mathbf{r_2}, ..., \mathbf{r_n})$ as the basic variable. In other words, all physical properties derivable from a given Hamiltonian through the solution of the time-independent Schrödinger equation are determined by $n(\mathbf{r})$. This includes the ground state energy $E[n(\mathbf{r})]$, among others. More precisely, all physical observables can in principle be expressed as functionals of the electronic charge-density.

The second major ingredient is the existence of a variational principle for the energy functional:

Theorem 2.1.2 (Hohenberg-Kohn 2,1964) *For any trial density* $n(\mathbf{r})$ *it holds* $E_0 \leq E[n(\mathbf{r})]$*, where* E_0 *is the ground-state energy for the system.*

In other words, the minimum value of the total-energy functional $E[n(\mathbf{r})]$ is the ground state energy of the system, and the density which yields its minimum value is exactly the single particle ground-state density.

The explicit form of this energy functional reads

$$E[n] = \int v(\mathbf{r})n(\mathbf{r})d\mathbf{r} + F[n], \tag{2.3}$$

where the universal functional

$$F[n] = \frac{1}{2}\iint \frac{n(\mathbf{r})n(\mathbf{r'})}{|\mathbf{r} - \mathbf{r'}|}d\mathbf{r}d\mathbf{r'} + G[n], \tag{2.4}$$

is often separated into the classical Coulomb term due to the charged electrons and the new universal functional $G[n]$.

2.1.2 Kohh-Sham theory

Although providing the ultimate theoretical foundation of DFT, the HK work of 1964 does not propose a simple way to solve the many-body problem. Such a scheme was in fact provided by the work of Kohn and Sham in 1965 [22]. The basic idea is to map the system of interacting electrons onto a non-interacting system with the same density, so that the problem can be cast in the form of single-particle equations. This is achieved in the spirit, and as an extension, of the Thomas-Fermi model, which can be considered the first density functional method.

Thomas-Fermi model

This first density-functional method was proposed independently by Thomas and Fermi in 1927 and 1928 [36][13]. The universal functional $F^{TF}[n(\mathbf{r})]$ is written as

$$F^{TF}[n] = C_F \int n(\mathbf{r})^{5/3} d\mathbf{r} + \frac{1}{2} \iint \frac{n(\mathbf{r})n(\mathbf{r}')}{|\mathbf{r}-\mathbf{r}'|} d\mathbf{r}d\mathbf{r}' \tag{2.5}$$

where the kinetic energy is approximated by that of a non-interacting homogeneous electron gas, and the Coulomb interaction by the Hartree term so that correlation is neglected.

The appealing feature of the Thomas-Fermi (TF) model is the fact that the energy functional is expressed explicitly in terms of the density by a simple one-to-one mapping. Unfortunately, although useful for obtaining qualitative trends, it should not be used when quantitative predictions on realistic systems are desired. The main explanations for its failures come from the inaccurate approximation of the kinetic energy as a density functional, since the kinetic energy is responsible for most of the total energy in a Coulombic system.

Kohn-Sham equations

The TF idea of obtaining the ground state kinetic energy from a non-interacting system is also the starting point for the Kohn-Sham (KS) scheme. For any interacting ground state density $n_0(\mathbf{r})$ construct a corresponding non-interacting system in some effective potential V_s such that the non-interacting Hamiltonian $H_s = T + V_s$ produce the same ground state density $n_0(\mathbf{r})$

$$E_s[n] = T_s[n] + \int v_s(\mathbf{r}) n(\mathbf{r}) d\mathbf{r}. \tag{2.6}$$

We know from the HK theory that

$$E[n] = \int v_{ext}(\mathbf{r}) n(\mathbf{r}) d\mathbf{r} + \frac{1}{2} \iint \frac{n(\mathbf{r})n(\mathbf{r}')}{|\mathbf{r}-\mathbf{r}'|} d\mathbf{r}d\mathbf{r}' + G[n] \tag{2.7}$$

$$= \int v_{ext}(\mathbf{r}) n(\mathbf{r}) d\mathbf{r} + U_H[n] + G[n], \tag{2.8}$$

and we now write the universal functional as

$$G[n] = T_s[n] + E_{xc}[n]. \tag{2.9}$$

where $T_s[n]$ is the kinetic energy of a system of non-interacting electrons with density $n(\mathbf{r})$ and $E_{xc}[n]$ is the definition of the exchange and correlation energy of the corresponding interacting system which we will discuss later.

The problem of minimizing the functional (2.7) is casted in the form of the Euler-Lagrange equation

$$\delta \left\{ E[n] - \mu \int n(\mathbf{r}) d\mathbf{r} \right\} = 0, \tag{2.10}$$

where the conservation of electrons is enforced by the Lagrange multiplier μ, fixed so that $\int n(\mathbf{r}) d\mathbf{r} = N$ Taking the functional derivatives and using (2.7) and (2.9) we obtain an expression for v_S

$$v_s(\mathbf{r}) = v_{ext}(\mathbf{r}) + \int \frac{n_0(\mathbf{r}')}{|\mathbf{r} - \mathbf{r}'|} d\mathbf{r}' + v_{xc}([n_0]; \mathbf{r}), \tag{2.11}$$

where the exchange and correlation potential is

$$v_{xc}([n_0]; \mathbf{r}) = \frac{\delta E_{xc}[n]}{\delta n(\mathbf{r})}\Big|_{n_0}. \tag{2.12}$$

Eq. (2.10) can then be rewritten as

$$\int \delta n(\mathbf{r}) \left\{ v_s(\mathbf{r}) + \frac{\delta T_s[n]}{\delta n(\mathbf{r})} \right\} d\mathbf{r} = 0, \tag{2.13}$$

which takes the same form of an equation applied to a system of non-interacting electrons moving in an effective potential $v_s(\mathbf{r})$. Therefore one obtains the sought density $n(\mathbf{r})$ by solving a set of single-particle Schrödinger equations for a given $v_s(\mathbf{r})$

$$\left[-\frac{1}{2}\nabla^2 + v_s(\mathbf{r}) \right] \phi_i(\mathbf{r}) = \epsilon_i \phi_i(\mathbf{r}), \tag{2.14}$$

and computing

$$n(\mathbf{r}) = \sum_{i=1}^{N} |\phi_i(\mathbf{r})|^2, \tag{2.15}$$

from which the ground state energy is

$$E_0 = \sum_{j}^{occ} \langle \phi_i | -\frac{1}{2}\nabla^2 | \phi_i \rangle + \int v_{ext}(\mathbf{r}) n(\mathbf{r}) d\mathbf{r} + U_H[n] + E_{xc}[n] \tag{2.16}$$

$$= T_s[\{\phi_i\}] + \int v_{ext}(\mathbf{r}) n(\mathbf{r}) d\mathbf{r} + U_H[n] + E_{xc}[n]. \tag{2.17}$$

As the sum of the eigenvalues in (2.14) is the same of the ground state energy of the non-interacting KS system in (2.6) we can rewrite the kinetic energy term $T_s[\{\phi_i\}]$ as

$$T_s[\{\phi_i\}] = \sum_{j}^{occ} \epsilon_j - \int v_s(\mathbf{r}) n(\mathbf{r}) d\mathbf{r}, \tag{2.18}$$

which allows to rewrite the ground state energy as

$$\begin{aligned} E_0 &= \sum_j^{occ} \epsilon_j - \frac{1}{2}\iint \frac{n(\mathbf{r})n(\mathbf{r}')}{|\mathbf{r}-\mathbf{r}'|} d\mathbf{r}d\mathbf{r}' + E_{xc}[n] - \int v_{xc}([n_0];\mathbf{r})n(\mathbf{r})d\mathbf{r} \\ &= \sum_j^{occ} \epsilon_j - U_H[n] + E_{xc}[n] - \int v_{xc}([n_0];\mathbf{r})n(\mathbf{r})d\mathbf{r}. \end{aligned} \tag{2.19}$$

Here are a few important remarks:

1. Although the KS equations are formally *exact*, the expression for the exchange and correlation energy is in general unknown and needs to be approximated. This also means that with the exact $E_{xc}[n]$ all many-body effects are in principle included.

2. In order to evaluate the total energies (2.16)-(2.19) the KS equations (2.14)are to be solved self-consistently, since the Kohn-Sham potential in turn depends on the density.

3. If one neglects $E_{xc}[n]$ and $v_{xc}([n_0];\mathbf{r})$ altogether the previous equations reduce to the self-consistent Hartree equations. Therefore the KS theory can be seen as a formal exactification of the Hartree approximation.

4. Neither the KS eigenstates ϕ_i nor eigenvalues ϵ_j have any obvious direct physical meaning except that the ϕ_i produce the true physical density by (2.15) and that the highest occupied ϵ_j equals the ionization potential.

2.1.3 Exchange and correlation

The exchange and correlations terms in the KS theory reflect the fact that the universal functional $F[n(\mathbf{r})]$ contains information beyond the Hartree term $U_H[n]$ and the one-body kinetic operator $T_s[\{\phi_i\}]$,

$$E_{xc}[n] = F[n(\mathbf{r})] - T_s[\{\phi_i\}] - U_H[n]. \tag{2.20}$$

In order to characterize it further it is usually separated into exchange and correlation components

$$E_{xc}[n] = E_x[n] + E_c[n]. \tag{2.21}$$

In analogy with the Hartree-Fock exchange energy, $E_x[n]$ is defined as that part of the interaction energy which is not included in the Hartree mean-field term, evaluated with respect to the non-interacting KS Slater determinant Φ_n^{min}

$$E_x[n] = \langle \Phi_n^{min} | V_{ee} | \Phi_n^{min} \rangle - U_H[n]. \tag{2.22}$$

The Hartree energy is just the classical electrostatic energy from a charge density $n(\mathbf{r})$, which also include a spurious self-interaction contribution, i.e. each orbital interacting with itself

$$U_H[n] = \frac{1}{2}\sum_{i,j}^{occ} \iint \frac{\phi_i^*(\mathbf{r})\phi_i(\mathbf{r})\phi_j^*(\mathbf{r}')\phi_j(\mathbf{r}')}{|\mathbf{r}-\mathbf{r}'|} d\mathbf{r}d\mathbf{r}'. \tag{2.23}$$

The exchange energy can also be written explicitly in terms of the KS orbitals

$$E_x[n] = -\frac{1}{2}\sum_{i,j}^{occ} \delta_{\sigma_i\sigma_j} \iint \frac{\phi_i^*(\mathbf{r})\phi_j(\mathbf{r})\phi_j^*(\mathbf{r}')\phi_i(\mathbf{r}')}{|\mathbf{r}-\mathbf{r}'|} d\mathbf{r}d\mathbf{r}', \tag{2.24}$$

which follows directly from the antisymmetry character of fermionic wavefunctions. Incidentally we notice that for $i = j$ the exchange contribution exactly cancels the self-interaction contribution from the Hartree term, as it is always the case in Hartree-Fock theory. The terms $i \neq j$ represent the Pauli repulsion by producing a large negative value of $E_x[n]$ for states with parallel spin and non-zero overlap.Physically it is due to the fact that two electrons with parallel spin tend to stay apart in space, thus lowering the total electrostatic energy with respect to the corresponding non-interacting system.

The correlation functional is defined as everything that is not accounted for by using a non-interacting Slater determinant, i.e. all extra information lacking in the KS wavefunctions and which has not been dealt with by exchange

$$E_c[n] = \langle \Psi_n^{min}|T + V_{ee}|\Psi_n^{min}\rangle - \langle \Phi_n^{min}|T + V_{ee}|\Phi_n^{min}\rangle \tag{2.25}$$

where Ψ_n^{min} is the true many-body wavefunction, i.e. the wavefunction which minimizes $T + V_{ee}$. By rewriting (2.25) as

$$\begin{aligned} E_c[n] = &\left(\langle \Psi_n^{min}|T|\Psi_n^{min}\rangle - \langle \Phi_n^{min}|T + V|\Phi_n^{min}\rangle\right) + \\ &\left(\langle \Psi_n^{min}|V_{ee}|\Psi_n^{min}\rangle - \langle \Phi_n^{min}|V_{ee}|\Phi_n^{min}\rangle\right) \end{aligned} \tag{2.26}$$

we see that the correlation energy contains many-body effects not included in the single-particle wavefunction of two types:

1. A kinetic contribution, which is positive since Φ_n^{min} is the wavefunction that minimizes T.

2. A potential correction, which is negative since the whole sum is negative.

They account for the fact that in the interacting system the electrons are kept apart due to the Coulomb repulsion, independently of the spin, thus lowering the electrostatic energy with respect to the non- interacting system and increasing the kinetic energy because of the restricted volume of space available.

2.2 Exchange and correlation functionals

For a DFT calculation to model real systems an accurate xc-functional must be used, which in practice has to be approximated. The formal definitions (2.22)-(2.26) do not provide much guidance for the approximation of their density functionals. This insight is provided by the adiabatic connection formula presented below. The section then continues with a discussion of the most used types of density functionals.

2.2.1 The Adiabatic Connection Formula

Let us define $0 < \lambda < 1$ as a coupling constant in $T + \lambda V_{ee}$ and $\Psi_n^{min\lambda}$ as the wavefunction which minimizes $T + \lambda V_{ee}$ still producing the ground state $n(\mathbf{r})$. Varying λ at fixed $n(\mathbf{r})$ corresponds to varying an external fictitious potential $v_\lambda(\mathbf{r})$ so that $\langle \Psi_n^{min\lambda} | \hat{n} | \Psi_n^{min\lambda} \rangle = n(\mathbf{r})$ is kept constant. This provides a smooth, "adiabatic connection" between the non-interacting and the true interacting ground states while λ increases from 0 to 1. When $\lambda = 0$, $\Psi_n^{min\lambda}$ equals Φ_n^{min}, i.e. the non-interacting Kohn-Sham wavefunction and the potential $v_\lambda(\mathbf{r})$ becomes the Kohn-Sham effective potential $v_s(\mathbf{r})$. When $\lambda = 1$, $\Psi_n^{min\lambda}$ equals Ψ_n^{min}, i.e. the true full interacting ground state and $v_\lambda(\mathbf{r})$ is the true external potential V_{ext}. Given this connection we can rewrite (2.26) as

$$\begin{aligned} E_{xc}[n] &= \langle \Psi_n^{min\lambda} | T + \ lambda V_{ee} | \Psi_n^{min\lambda} \rangle \Big|_{\lambda=1} - \langle \Psi_n^{min\lambda} | T + V_{ee} | \Psi_n^{min\lambda} \rangle \Big|_{\lambda=0} - U[n] \\ &= \int_0^1 \frac{d}{d\lambda} \langle \Psi_n^{min\lambda} | T + \lambda V_{ee} | \Psi_n^{min\lambda} \rangle \, d\lambda - U[n] \end{aligned} \tag{2.27}$$

The Hellmann-Feynman theorem allows us to simplify (2.27) to

$$E_{xc}[n] = \int d\lambda \, \langle \Psi_n^{min\lambda} | V_{ee} | \Psi_n^{min\lambda} \rangle - U[n] \tag{2.28}$$

where we notice that the kinetic contribution to $E_{xc}[n]$ has been absorbed in the coupling-constant integration.

In order to evaluate the N-electron expectation value of the two-body operator V_{ee} in (2.28) we introduce the two-electron reduced density matrices ρ_2

$$\rho_2(\mathbf{r}', \mathbf{r}) = N(N-1) \int d\mathbf{r}_3 \ldots \int d\mathbf{r}_N |\Psi(\mathbf{r}', \mathbf{r}, \ldots, \mathbf{r}_N)|^2 \tag{2.29}$$

so that we get

$$\langle V_{ee} \rangle = \frac{1}{2} \int d\mathbf{r} \int d\mathbf{r}' \frac{\rho_2(\mathbf{r}', \mathbf{r})}{|\mathbf{r} - \mathbf{r}'|} \tag{2.30}$$

from which we interpret the number $\rho_2(\mathbf{r}', \mathbf{r})$ as the joint probability of finding an electron in the volume element $d\mathbf{r}'$ at position $\mathbf{r}'$ an electron in $d\mathbf{r}$ at $\mathbf{r}$. This is then equivalent to

$$\rho_2(\mathbf{r}', \mathbf{r}) = n(\mathbf{r}) n_2(\mathbf{r}, \mathbf{r}') \tag{2.31}$$

where $n_2(\mathbf{r}, \mathbf{r}')$ is the conditional probability for finding an electron at $\mathbf{r}'$ given that there is one at $\mathbf{r}$. For the wavefunction $\Psi_n^{min\lambda}$ we write n_2 as

$$n_2(\mathbf{r}, \mathbf{r}') = n(\mathbf{r}') + n_{xc}^{\lambda}(\mathbf{r}, \mathbf{r}') \tag{2.32}$$

thus defining the exchange and correlation hole $n_{xc}^{\lambda}(\mathbf{r}, \mathbf{r}')$, which can be easily shown to satisfy the sum rule

$$\int n_{xc}^{\lambda}(\mathbf{r}, \mathbf{r}') d\mathbf{r}' = -1 \tag{2.33}$$

which represents the missing of one electron, namely the one at $\mathbf{r}$. We can then rewrite 2.28 as

$$E_{xc}[n] = \frac{1}{2} \int d\mathbf{r} \int d\mathbf{r}' \frac{n(\mathbf{r}) \overline{n}_{xc}(\mathbf{r}, \mathbf{r}')}{|\mathbf{r} - \mathbf{r}'|} \tag{2.34}$$

where

$$\overline{n}_{xc}(\mathbf{r}, \mathbf{r}') = \int_0^1 d\lambda n_{xc}^{\lambda}(\mathbf{r}, \mathbf{r}') \tag{2.35}$$

is the coupling-constant averaged hole density. From 2.35 we the interpret the exchange-correlation energy as the electrostatic interaction between the electrons and the averaged xc-hole which surrounds it.

If we consider the limit $\lambda = 0$ we can define the exchange-hole density as

$$n_x = n_{xc}^{\lambda=0}(\mathbf{r}, \mathbf{r}') \tag{2.36}$$

which can be constructed explicitly from the KS orbitals since $\Psi_n^{min\lambda=0}$ is now a KS Slater determinant.

2.2.2 Approximations for XC

Equation (2.34) for $E_{xc}[n]$ can be rewritten as

$$E_{xc}^{LDA}[n(\mathbf{r})] = \int d\mathbf{r} n(\mathbf{r}) \varepsilon_{xc}(\mathbf{r}, [n(\tilde{\mathbf{r}})]) \tag{2.37}$$

where $\varepsilon_{xc}(\mathbf{r}, [n(\tilde{\mathbf{r}})])$ represents an exchange-correlation energy per particle at point $\mathbf{r}$, which is also a functional of the density $n(\tilde{\mathbf{r}})$. The most common and traditional approximations for $E_{xc}[n]$ have a quasi local form, i.e. they depends primarily on he density $n(\tilde{\mathbf{r}})$ at points $\tilde{\mathbf{r}}$ near $\mathbf{r}$, where "near" is a microscopic distance such as the local Fermi wavelength or the TF screening length.

LDA

The Local Density Approximation, introduced by Kohn and Sham in ([22]), approximates $\varepsilon_{xc}(\mathbf{r}, [n(\tilde{\mathbf{r}})])$ by that of an homogeneous electron gas with the same density as the local density of the real system $n(\mathbf{r})$

$$E_{xc}^{LDA}[n(\mathbf{r})] = \int d\mathbf{r} n(\mathbf{r}) \varepsilon_{xc}^{unif}(\mathbf{r}, [n(\tilde{\mathbf{r}})]) \tag{2.38}$$

The exchange part can written analytically from (2.24), where the KS orbitals are plane-waves since the KS potential v_s in constant in for an homogeneous electron gas

$$\varepsilon_x^{unif}(n) = -\frac{3}{4\pi}(3\pi^2 n)^{1/3} \tag{2.39}$$

Analytical expressions for the correlation part ε_c^{unif} are only known in certain limits, and one then uses expression fitted from accurate quantum Monte-Carlo calculations. The most common parametrizations are the Perdew-Wang [29] and the Perdew-Zunger [30].

By construction LDA is exact for a uniform electron gas, and it's then expected to be a good approximation for densities varying sufficiently slowly. Nevertheless the LDA has proven to yield good results in most applications, even for atomic systems where the hypotesis of constant density is evidently violated. This has been at least in part attributed to the fact that the LDA shows many formal features, such as the sum rule for the exchange-correlation hole. However, though surprisingly good if compared to the simplicity of the approximation, the LDA has several fundamental failures such as unwanted self-interactions.

A slightly more complex version of LDA is the Local-Spin-Density Approximation (LSDA), which includes information about the local density of each spin.

$$E_{xc}^{LSDA} = \int d\mathbf{r} n(\mathbf{r}) \varepsilon_{xc}(n_\downarrow(\mathbf{r}), n_\uparrow(\mathbf{r})) \tag{2.40}$$

The LSDA performs significantly better for system with some spin-polarization.

GGA

Although LDA is still the common choice in solid state physics, several Generalized Gradient Approximations (GGA) have pushed LDA results to the accuracy usually required by the quantum chemistry community.

The first obvious step beyond the local approximation is a functional of both the density $n(\mathbf{r})$ and the magnitude of its gradient $|\nabla n|$, as it was suggested already in the original paper [22]. However, such a gradient expansion does not provide consistent and systematic improvements over the LDA, the main problem being the fact that gradients in real materials can

be so large that the expansion breaks down. Indeed it violates many formal conditions, often producing worse results. It is convenient to define the functional as a generalized form of (2.38)

$$\begin{aligned} E_{xc}^{GGA} &= \int d\mathbf{r}\varepsilon_{xc}^{GGA}(n(\mathbf{r}), |\nabla n(\mathbf{r})|) \\ &\equiv \int d\mathbf{r}\varepsilon_{xc}^{unif}(n(\mathbf{r}))F_{xc}(n(\mathbf{r}), |\nabla n(\mathbf{r})|) \end{aligned} \tag{2.41}$$

where F_{xc} is a dimensionless enhancement factor and ε_x^{unif} is the exchange energy of an homogeneous electron gas, same as in the LDA.

The exchange energy, common for all GGAs, is written as

$$E_x^{GGA} = \int d\mathbf{r}n(\mathbf{r})\varepsilon_x^{unif}(n(\mathbf{r}))F_x(s) \tag{2.42}$$

where

$$s = \frac{|\nabla n(\mathbf{r})|}{2k_f n(\mathbf{r})} \tag{2.43}$$

is a dimensionless reduced density gradient, i.e. a measure of how fast and how much the density varies on the scale of the Fermi wavelength. Different exchange GGAs only differ for the enhancement factor $F_x(s)$, for which various forms have been proposed; the most widely used are by Becke (B88) [4], Perdew and Wang (PW91) [29]and Perdew, Burke and Enzerhof (PBE) [10]. Revised versions of PBE have also been proposed, such as revPBE [37]and RPBE [14].

The correlation part is generally more difficult, but its contribution to the total energy is also typically much smaller than the exchange.

Hybrid Functionals

The observation that $\lambda = 0$ in the coupling constant integration corresponds to the exact HF exchange energy suggests to mix a fraction of exact exchange with the GGA (or LDA) exchange and correlation

$$E_{xc}^{hyb} = aE_x^{exact} + (1-a)E_x^{GGA} + E_c^{GGA} \tag{2.44}$$

where the parameter a can be either fitted empirically from atomic and molecular databases or it can be estimated theoretically.

Several parametrizations are available in literature, one of the most famous on being the B3LYP

$$E_{xc}^{B3LYP} = E_x^{LDA} + a_0(E_x^{exact} - E_x^{GGA}) + a_x E_x^{B88} + a_c E_c^{LYP} \tag{2.45}$$

with the coefficient adjusted to fit atomic and molecular data, and correlation treated used the Lee-Yang-Parr (LYP) [24].

Hybrid functionals are today the most accurate functionals as far as energetics is concerned, and are the method of choice in quantum chemical calculations.

Orbital-Dependent Functionals

A broad class of approximations tries to improve the exchange and correlation functionals by expressing $E_{xc}[n]$ explicitly in terms of the Kohn-Sham orbitals ϕ_i. This could be rationalized by noting that the main advance of the Kohn-Sham approach over the Thomas-Fermi method is indeed the expression of the kinetic energy in terms of the single-particle orbitals. When this idea is applied to the exchange part of $E_{xc}[n]$, the approximation is denoted as "exact exchange" (EXX), but general approaches applicable to correlation functionals do exist as well.

Another line of approximations which makes use of orbital-dependent functionals tries to correct for the unphysical self-interaction present in many exchange and correlation functionals. This problem is most important in system with localized or strongly interacting electrons. Two of these methods are SIC and LDA+U.

Chapter 3

Projector Augmented Wave Method

In order to solve the electronic structure problem within the DFT formalism, the Kohn-Sham equations are to be solved in some efficient numerical way.

One of the main issues in condensed matter systems is the very different behaviour of the wavefunction at different distances from the nuclei. Since the atomic wavefunctions are eigenstates of the atomic Hamiltonian, they must be all mutually orthogonal. Since the core states are well localized around the nucleus, the valence state must oscillate rapidly in the core region in order to mantain this orthogonality, making it difficult to describe them accurately without using a very large basis set, or a very fine mesh. On the other hand, the core electrons are practically inert and very localized, and only the valence electrons contribute to the chemical behaviour of a given specie. This argument then suggests to treat core and valence electrons in a different way, possibly obtaining numerical advantages.

One common approach is the use of "pseudopotentials" in which nuclei and core electrons are described by an effective, smooth potential, which is constructed in such a way to reproduce the correct effect on the remaining valence electrons. The Kohn-Sham equations are then solved only for the valence electrons, thus reducing the computational effort; the pseudopotentials are calculated and tabulated once for each element. On the other hand, all information about the real wavefunction close to the nuclei is lost, making it hard to compute properties which rely on the core region (electric field gradients, hyperfine parameters, etc). A second major drawback is that there is no systematic way to generate good pseudopotentials, so the procedure is not well controlled.

Another approach is the so called class of "all-electron" methods, in which the full information about the wavefunction is available. This approach is usually tied to the frozen-core approximation, in which the core orbitals are calculated and tabulated once and held fixed. This is again

justified by the fact that the core states are not influenced by the chemical environment, at least for most purposes. One of the most important of such methods is the Augmented-Plane-Wave method (APW), in which the space is partitioned in two regions: a spherical one around each atom in which the wavefunction is expanded onto a local basis in order to reproduce the great variations, and an interstitial region in which another basis is chosen (plane waves for instance) and connected to the first local basis.

A more general approach is the Projector-Augmented-Wave method (PAW) introduced by Blöchl in 1994 [5] as an extension of both augmented-wave and pseudopotential methods, which in fact can be recovered by well defined approximations [28] [23]. This method is presented in this chapter, since all the work contained in this thesis is done within this formalism, which is implemented in a state-of-the-art real space code GPAW [17].

3.1 PAW Transformation Operator

As mentioned above, the shape of the wavefunctions is very different in different regions of space. The basic idea of the PAW method is to divide the wavefunction into two parts: a partial wave expansion within an atom-centered sphere, and an envelope function outside. The two parts are then matched smoothly at the sphere edge.

We seek a linear transformation $\hat{\mathcal{T}}$ which maps some computationally convenient ("pseudo" (PS) or "smooth") wavefunctions $|\tilde{\psi}\rangle$ to the physically relevant ("true" or "all-electron") wavefunctions $|\psi\rangle$

$$|\psi_n\rangle = \hat{\mathcal{T}}\,|\tilde{\psi}_n\rangle \tag{3.1}$$

where n is a quantum state label, consisting of a band index and possibly a spin and $\mathbf{k}$-vector index. The ground state PS wave function is then obtained by solving the Kohn-Sham equations in the transformed Hilbert space

$$\hat{\mathcal{T}}^\dagger \hat{H} \hat{\mathcal{T}}\,|\tilde{\psi}_n\rangle = \epsilon_n \hat{\mathcal{T}}^\dagger \hat{\mathcal{T}}\,|\tilde{\psi}_n\rangle \tag{3.2}$$

Since the true wavefunctions are smooth enough at a certain distance from the core, we require that the transformation is just the unity operator beyond the augmentation cut-off and a sum of atom-centered contributions inside

$$\hat{\mathcal{T}} = 1 + \sum_a \hat{\mathcal{T}}^a \tag{3.3}$$

where a is an atom index and $\hat{\mathcal{T}}^a = \hat{\mathcal{T}}^a(\mathbf{r} - \mathbf{R^a}) = 0$ for $|\mathbf{r} - \mathbf{R^a}| > r_c^a$. The cut-off radii r_c^a is chosen such that there is no overlap between augmentation spheres.

Within the augmentation region $\mathbf{\Omega_a}$, we expand the PS wavefunction into PS partial waves $\tilde{\phi}^a$

$$|\tilde{\psi}_n\rangle = \sum_{ia} c_{ni}^a\,|\tilde{\phi}_i^a\rangle \;\text{ within } \mathbf{\Omega_a} \tag{3.4}$$

and similarly its all-electron counterpart via eq.(3.1)

$$|\psi_n\rangle = \sum_{ia} c^a_{ni} \, |\phi^a_i\rangle \;\; \text{within } \mathbf{\Omega_a} \tag{3.5}$$

By applying eq.(3.1) we obtain

$$|\phi^a_i\rangle = (1 + \hat{\mathcal{T}}^a) \, |\tilde{\phi}^a_i\rangle \;\Rightarrow\; \hat{\mathcal{T}}^a \, |\tilde{\phi}^a_i\rangle = |\phi^a_i\rangle - |\tilde{\phi}^a_i\rangle \quad \forall a, i \tag{3.6}$$

which fully determines the transformation $\hat{\mathcal{T}}$ in terms of the partial waves. Hence we can express the true wavefunction as

$$|\psi_n\rangle = |\tilde{\psi}_n\rangle - \sum_{ia} c^a_{ni} \, |\tilde{\phi}^a_i\rangle + \sum_{ia} c^a_{ni} \, |\phi^a_i\rangle \tag{3.7}$$

with the expansion coefficients to be determined.

Since we require $\hat{\mathcal{T}}$ to be linear, the coefficients must be linear functionals of the PS wavefunction $|\tilde{\psi}_n\rangle$, i.e. scalar products

$$c^a_{ni} = \langle \tilde{p}^a_i | \tilde{\psi}_n \rangle \equiv P^a_{ni} \tag{3.8}$$

where $\tilde{p}^a_i$ are some fixed functions, named PS projector functions, and the name P^a_{ni} is given for consistence with existing literature.

If we require zero overlap between different augmentation spheres, the one-center expansion of a PS wavefunction $\sum_i \langle \tilde{p}^a_i | \tilde{\psi}_n \rangle \, |\tilde{\phi}^a_i\rangle$ has to be identical to $|\tilde{\phi}^a_i\rangle$ itself inside the augmentation sphere. This is equivalent to fulfilling the completeness relation

$$\sum_i |\tilde{\phi}^a_i\rangle \, \langle \tilde{p}^a_i| = 1 \quad \text{within } \mathbf{\Omega}_a \tag{3.9}$$

which in turn implies that

$$\langle \tilde{p^a_{i_1}} | \tilde{\phi^a_{i_2}} \rangle = \delta_{i_1, i_2} \quad \text{within } \mathbf{\Omega}_a \tag{3.10}$$

i.e. PS projector functions and partial waves are mutually orthonormal within the augmentation sphere.

Finally, by inserting (3.8) into (3.7) we obtain a closed form for the transformation operator

$$\hat{\mathcal{T}} = \sum_a \sum_i (|\phi^a_i\rangle - |\tilde{\phi}^a_i\rangle) \, \langle \tilde{p}^a_i| \tag{3.11}$$

which allows us to get the true, all-electron, Kohn-Sham wavefunction $\psi_n(\mathbf{r}) = \langle \mathbf{r} | \psi_n \rangle$ as

$$\psi_n(\mathbf{r}) = \tilde{\psi}_n(\mathbf{r}) + \sum_a \sum_i (\phi^a_i(\mathbf{r}) - \tilde{\phi}^a_i(\mathbf{r})) \, \langle \tilde{p}^a_i | \tilde{\psi}_n \rangle \tag{3.12}$$

It is generally convenient to introduce the one center expansions

$$\begin{aligned} \psi_n^a(\mathbf{r}) &= \sum_i \phi_i^a(\mathbf{r}) \langle \tilde{p}_i^a | \tilde{\psi}_n \rangle \\ \tilde{\psi}_n^a(\mathbf{r}) &= \sum_i \tilde{\phi}_i^a(\mathbf{r}) \langle \tilde{p}_i^a | \tilde{\psi}_n \rangle \end{aligned} \tag{3.13}$$

which makes it possible to write the true wavefunction compactly as

$$\psi_n(\mathbf{r}) = \tilde{\psi}_n(\mathbf{r}) + \sum_a (\psi_n^a(\mathbf{r}) - \tilde{\psi}_n^a(\mathbf{r})) \tag{3.14}$$

explicitly separating the extended-space and the atom-centered contributions. This will often be exploited to obtain compact expression for various quantities in PAW. The first term can be evaluated on an extended grid, or on a soft basis-set, while the last two terms are evaluated on fine radial grids.

In summary, the three ingredients that determine the PAW transformation are:

a) The partial waves ϕ_i^a, which are constructed as solutions of the Schrodinger equation for the isolated atom and used as an atomic basis for the all-electron wavefunctions within the augmentation sphere.

b) The PS (smooth) partial waves $\tilde{\phi}_i^a$, which coincide with the corresponding true partial waves outside the augmentation sphere but are smooth continuations inside the spheres. These are used as atomic basis-sets for the PS wavefunctions.

c) The PS (smooth) projector functions $\tilde{p}_i^a$, one for each partial wave, which fulfill the condition $\langle \tilde{p}_{i_1}^a | \tilde{\phi}_{i_2}^a \rangle = \delta_{i_1,i_2}$ inside each augmentation sphere.

3.2 Approximations

Up to this point the PAW method appears as an exact implementation of the density functional theory. In order to make it a practical scheme, some approximations are needed.

Frozen Core

The frozen core approximation assumes that the core states are localized in the augmentation spheres and that the core states are not modified by the chemical environment. The core Kohn-Sham states are thus chosen to be exactly the core states of the isolated atoms:

$$|\phi_n^c\rangle = |\psi_\alpha^{a,core}\rangle \tag{3.15}$$

Notice that, differently from (3.5), no projector functions needs to be defined for the core states.

Finite basis set

The extended PS contribution $\tilde{\psi}_n$ in (3.14) is evaluated outside the augmentation spheres by means of a suitable basis set or on a real-space grid. In both cases the non completeness of the basis, or equivalently the finite grid-spacing, will introduce an error.

Finite number of partial waves and projectors

The number of partial waves and projector functions is obviously finite. This means that that the completeness conditions we have required are not strictly fulfilled. However the approximation can be controlled by increasing the number of partial waves and projectors so that they form a satisfactory complete space for the expansion of the wavefunctions within the augmentation spheres.

3.3 Expectation values

In order to evaluate physical observables we need to evaluate expectation values of some operator A, which we can express both in terms of PS wavefunctions or true wavefunction. Within the frozen core approximation, it reads

$$\begin{aligned}\langle A\rangle &= \sum_n^{val} f_n \langle\psi_n|A|\psi_n\rangle + \sum_a \sum_\alpha^{core} \langle\phi_\alpha^{a,core}|A|\phi_\alpha^{a,core}\rangle \\ &= \sum_n^{val} f_n \langle\tilde{\psi}_n|\tilde{A}|\tilde{\psi}_n\rangle + \sum_a \sum_\alpha^{core} \langle\phi_\alpha^{a,core}|\tilde{A}|\phi_\alpha^{a,core}\rangle\end{aligned} \tag{3.16}$$

The PAW-transformed operator $\tilde{A}$ is obtained from (3.1)

$$\begin{aligned}\tilde{A} &= \hat{\mathcal{T}}^\dagger A \hat{\mathcal{T}} \\ &= A + \sum_a \sum_{i_1,i_2} |\tilde{p}_{i_1}^a\rangle \left(\langle\phi_{i_1}^a|A|\tilde{\phi}_{i_2}^a\rangle - \langle\tilde{\phi}_{i_1}^a|A|\phi_{i_2}^a\rangle\right) \langle\tilde{p}_{i_2}^a| + \Delta A^{NL}\end{aligned} \tag{3.17}$$

where

$$\begin{aligned}\Delta A^{NL} = &\sum_{a,i_1} |\tilde{p}_{i_1}^a\rangle \left(\langle\phi_{i_1}^a| - \langle\tilde{\phi}_{i_1}^a|\right) A \left(1 - \sum_{a',i_2} |\tilde{\phi}_{i_2}^{a'}\rangle \langle\tilde{p}_{i_2}^{a'}|\right) \\ &+ \left(1 - \sum_{a',i_2} |\tilde{p}_{i_2}^{a'}\rangle \langle\tilde{\phi}_{i_2}^{a'}|\right) A \sum_{a,i_1} \left(|\phi_{i_1}^a\rangle - |\tilde{\phi}_{i_1}^a\rangle\right) \langle\tilde{p}_{i_1}^a|\end{aligned} \tag{3.18}$$

is the non-local contribution, which is non-zero only if A is a non-local operator in coordinate representation. If A is local ΔA^{NL} vanishes because $\sum_{a',i_2} |\tilde{\phi}^{a'}_{i_2}\rangle \langle \tilde{p}^{a'}_{i_2}| = 1$ inside the augmentation spheres, while $\langle \phi^a_{i_1}| - \langle \tilde{\phi}^a_{i_1}|$ is zero outside the spheres.

By using (3.17), we can now write the expectation value of a local operator A as

$$\langle A \rangle = \sum_n^{val} f_n \langle \tilde{\psi}_n|A|\tilde{\psi}_n\rangle + \sum_a \sum_{i_1,i_2} \sum_n f_n \langle \tilde{\psi}_n|\tilde{p}^a_{i_1}\rangle \left(\langle \phi^a_{i_1}|A|\tilde{\phi}^a_{i_2}\rangle - \langle \tilde{\phi}^a_{i_1}|A|\phi^a_{i_2}\rangle \right) \langle p^{\tilde{a}}_{i_2}|\tilde{\psi}_n\rangle + \\ + \sum_a \sum_\alpha^{core} \langle \phi^{a,core}_\alpha|A|\phi^{a,core}_\alpha\rangle \tag{3.19}$$

By introducing the one-center density matrix

$$D^a_{i_1 i_2} = \sum_n f_n \langle \tilde{\psi}_n|\tilde{p}^a_{i_1}\rangle \langle p^{\tilde{a}}_{i_2}|\tilde{\psi}_n\rangle = \sum_n f_n P^{a*}_{ni_1} P^a_{ni_2} \tag{3.20}$$

we can finally cast (3.19) into

$$\langle A \rangle = \sum_n^{val} f_n \langle \tilde{\psi}_n|A|\tilde{\psi}_n\rangle + \sum_a \sum_{i_1,i_2} \left(\langle \phi^a_{i_1}|A|\tilde{\phi}^a_{i_2}\rangle - \langle \tilde{\phi}^a_{i_1}|A|\phi^a_{i_2}\rangle \right) D^a_{i_1 i_2} + \\ + \sum_a \sum_\alpha^{core} \langle \phi^{a,core}_\alpha|A|\phi^{a,core}_\alpha\rangle \tag{3.21}$$

For future convenience we notice that by making use of the one-center expansion of eq.(3.13) we can also write

$$\langle A \rangle = \sum_n^{val} f_n (\langle \tilde{\psi}_n|A|\tilde{\psi}_n\rangle + \sum_a (\langle \phi^a_n|A|\psi^a_n\rangle - \langle \tilde{\phi}^a_n|A|\tilde{\psi}^a_n\rangle)) + core \tag{3.22}$$

where the core contribution takes the same form as the valence expression.

3.3.1 Density

The charge density at point $\mathbf{r}$ is the expectation value of the real-space projection operator $|\mathbf{r}\rangle \langle \mathbf{r}|$

$$n(\mathbf{r}) = \sum_n f_n \langle \psi_n|\mathbf{r}\rangle \langle \mathbf{r}|\psi_n\rangle = \sum_n f_n |\psi_n(\mathbf{r})|^2 \tag{3.23}$$

Since it is a local operator, we can directly apply either (3.21) or (3.22) and get

$$n(\mathbf{r}) = \tilde{n(\mathbf{r})} + \sum_a (n^a(\mathbf{r}) - \tilde{n^a}(\mathbf{r})) \tag{3.24}$$

where

$$\begin{aligned} \tilde{n(\mathbf{r})} &= \sum_n f_n |\tilde{\psi}_n(\mathbf{r})|^2 + \tilde{n_c(\mathbf{r})} \\ n^a(\mathbf{r}) &= \sum_{i_1 i_2} D^a_{i_1 i_2} \phi^a_{i_1}(\mathbf{r}) \phi^a_{i_2}(\mathbf{r}) + n^a_c(\mathbf{r}) \\ \tilde{n^a(\mathbf{r})} &= \sum_{i_1 i_2} D^a_{i_1 i_2} \tilde{\phi^a_{i_1}}(\mathbf{r}) \tilde{\phi^a_{i_2}}(\mathbf{r}) + \tilde{n^a_c}(\mathbf{r}). \end{aligned} \tag{3.25}$$

Notice that by introducing the pseudo core density $\tilde{n^a_c}$, we implicitly take into account possible contributions from core states which extends outside the augmentation spheres.

3.4 Total Energy

The total energy is given by the DFT expression (2.16). Symbolically it reads

$$E[n] = T_s[n] + U_H[n] + V_{ext}[n] + E_{xc}[n] \tag{3.26}$$

Like wavefunctions and expectation values, we also want the total energy to be be separated into three contributions

$$E = \tilde{E} + \sum_a (E^a - \tilde{E}^a) \tag{3.27}$$

where, as usual, the first one only contains smooth functions and is spatially extended while the last two contributions are atom-centered corrections. The goal is thus to obtain an expression with no terms which need to be evaluated on two incompatible grids.

3.4.1 Kinetic energy

The kinetic energy term is usually written as an explicit functional of the Kohn-Sham orbitals (it is still an implicit functional of the density as well)

$$T_s[\{\psi_n\}] = \sum_n f_n \left\langle \psi_n \right| -\frac{1}{2}\nabla^2 \left| \psi_n \right\rangle . \tag{3.28}$$

Since it is a (semi-) local functional, it can be easily separated by applying (3.21) directly to get

$$T_s[\{\psi_n\}] = \tilde{T}_s + \sum_a (T^a_s - \tilde{T}^a_s) \tag{3.29}$$

where

$$\begin{aligned} T_s &= \sum_n f_n \langle\tilde{\psi}_n| - \frac{1}{2}\nabla^2|\tilde{\psi}_n\rangle \\ T_s^a &= D^a_{i_1 i_2} \langle\phi^a_{i_1}| - \frac{1}{2}\nabla^2|\phi^a_{i_2}\rangle + \sum_\alpha^{core} \langle\phi^{a,core}_\alpha| - \frac{1}{2}\nabla^2|\phi^{a,core}_\alpha\rangle \\ \tilde{T_s^a} &= D^a_{i_1 i_2} \langle\tilde{\phi^a_{i_1}}| - \frac{1}{2}\nabla^2|\tilde{\phi^a_{i_2}}\rangle + \sum_\alpha^{core} \langle\tilde{\phi^{a,core}_\alpha}| - \frac{1}{2}\nabla^2|\tilde{\phi^{a,core}_\alpha}\rangle \end{aligned} \tag{3.30}$$

3.4.2 Exchange and Correlation energy

As long as semi-local approximations are considered, such as LDAs or GGAs, equation (3.21) can be used to obtain

$$E_{xc}[n] = E_{xc}[\tilde{n}] + \sum_a (E_{xc}[n^a] - E_{xc}[\tilde{n^a}]) \tag{3.31}$$

The atom-centered correction can be written as a functional of the density matrix defined in (3.20) through (3.25)

$$E_{xc}[n^a] - E_{xc}[\tilde{n^a}] = \Delta E_{xc}[\{D^a_{i_1 i_2}\}] \tag{3.32}$$

3.4.3 Hartree energy

In the term $U_H[n]+V_{ext}[n]$ from the total energy, the external potential V_{ext} is the sum of the potential from the nuclei, of charge $Z^a(\mathbf{r}) = -\mathcal{Z}\delta(\mathbf{r}-\mathbf{R}^a)$, and of any other actual external fields. In the following we will assume that the latter contribution is strictly zero. We are then left with

$$\begin{aligned} U_H^{tot} &\equiv U_H[n] + V_{ext}[n] \\ &= \frac{1}{2}\iint \frac{n(\mathbf{r})n(\mathbf{r}')}{|\mathbf{r}-\mathbf{r}'|} d\mathbf{r}d\mathbf{r}' + \iint \frac{n(\mathbf{r})\sum_a Z^a(\mathbf{r}')}{|\mathbf{r}-\mathbf{r}'|} d\mathbf{r}d\mathbf{r}' + \\ &\quad + \frac{1}{2}\sum_{a\neq a'} \iint \frac{Z^{a'}(\mathbf{r})Z^a(\mathbf{r}')}{|\mathbf{r}-\mathbf{r}'|} d\mathbf{r}d\mathbf{r}' \end{aligned} \tag{3.33}$$

which I will call total the Hartree energy, as it represents the total electrostatic energy of the system, i.e. nuclei and electrons. In fact, by introducing the charge neutral total density $\rho(\mathbf{r}) = n(\mathbf{r}) + \sum_a Z^a(\mathbf{r})$ it can be written as

$$U_H^{tot}[n] \simeq U_H[\rho] = \iint \frac{\rho(\mathbf{r})\rho(\mathbf{r}')}{|\mathbf{r}-\mathbf{r}'|} d\mathbf{r}d\mathbf{r}' \tag{3.34}$$

the symbol $\simeq$ being due to the fact that the Hartree total energy of the right-hand side introduces a self-interaction term for the nuclei. This behaviour must be removed obviously, as we will show later.

In order to separate the extended pseudo part and the one-center part, we add and subtract from the total density a compensation charge $\tilde{Z}^a$ inside the augmentation spheres

$$\rho = n + \sum_a (Z^a + \tilde{Z}^a - \tilde{Z}^a) \tag{3.35}$$

and by expanding n according to (3.24) we obtain

$$\rho = \tilde{\rho} + \sum_a (\rho^a - \tilde{\rho^a}) \tag{3.36}$$

where

$$\begin{aligned} \tilde{\rho} &= \tilde{n} + \sum_a \tilde{Z}^a \\ \rho^a &= n^a + Z^a \\ \tilde{\rho^a} &= \tilde{n^a} + \tilde{Z}^a \end{aligned} \tag{3.37}$$

The Hartree energy can then be written as a sum of the usual three contributions

$$U_H = U[\tilde{\rho}] + \sum_a (U[\rho^a] U[\tilde{\rho^a}]) \tag{3.38}$$

where

$$\begin{aligned} U[\tilde{\rho}] &= \frac{1}{2} \iint \frac{\tilde{\rho}(\mathbf{r})\tilde{\rho}(\mathbf{r}')}{|\mathbf{r} - \mathbf{r}'|} d\mathbf{r} d\mathbf{r}' \\ U[\rho^a] &= \frac{1}{2} \iint \frac{\rho^a(\mathbf{r})\rho^a(\mathbf{r}')}{|\mathbf{r} - \mathbf{r}'|} d\mathbf{r} d\mathbf{r}' \\ U[\tilde{\rho}^a] &= \frac{1}{2} \iint \frac{\tilde{\rho}^a(\mathbf{r})\tilde{\rho}^a(\mathbf{r}')}{|\mathbf{r} - \mathbf{r}'|} d\mathbf{r} d\mathbf{r}' \end{aligned} \tag{3.39}$$

Notice that the problem of the nuclear self-interaction in (3.34) is solved automatically in the PAW formalism, i.e. it is taken care of by the atom-centered contributions. The contribution $U[\tilde{\rho}]$ in (3.38) is, in fact, a Hartree term without any self-interaction corrections.

Compensation charges

The compensation charges $\tilde{Z}^a$ are introduced so that also the Hartree energy can be separated into the extended smooth part and the atom-centered correction. This means that the atom-centered correction $\rho^a - \tilde{\rho}^a$ should not interact with charges outside the augmentation spheres, i.e. it should have vanishing electrostatic multipole moments. In other words, we require the pseudo charge density $\tilde{\rho}$ to have the same multipole moments as the all-electron charge density ρ. The potential from a localized charge distribution seen from outside the region of localization, in fact, only depends

on the multipole moments and not on the actual geometry of the charge distribution. This requirement is expressed as

$$\int d\mathbf{r} r^l (\rho^a - \tilde{\rho}^a) Y_L(\mathbf{r} - \mathbf{R}^a) = 0 \tag{3.40}$$

where $L = (l, m)$ is the angular and magnetic index of the spherical harmonics expansion Y_L

It is thus natural to construct the compensation charges by multipole expansion of localized smooth functions $\tilde{g}_L^a$

$$\tilde{Z}^a = \sum_L Q_L^a \tilde{g}_L^a(\mathbf{r}) \tag{3.41}$$

where the functions $\tilde{g}_L^a$ are normalized as

$$\int d\mathbf{r} r^l \tilde{g}_L^a(\mathbf{r}) Y_L(\mathbf{r} - \mathbf{R}^a) = 1 \tag{3.42}$$

By inserting (3.41) into (3.40) we find an expression for the multipole moments

$$\begin{aligned} Q_L^a &= d\mathbf{r} r^l [n^a(\mathbf{r}) + Z^a(\mathbf{r}) - \tilde{n}^a(\mathbf{r})] Y_L(\mathbf{r} - \mathbf{R}^a) \\ &= \Delta^a \delta_{l,0} + \sum_{i_1 i_2} \Delta^a_{L,i_1 i_2} D^a_{i_1 i_2} \end{aligned} \tag{3.43}$$

where

$$\begin{aligned} \Delta^a &= \int d\mathbf{r} Y_{00}(\hat{\mathbf{r}}) [n_c^a(\mathbf{r}) - \tilde{n}_c^a(\mathbf{r}) - \mathcal{Z}^a \delta(\mathbf{r})] \\ \Delta^a_{L,i_1 i_2} &= \int d\mathbf{r} r^l Y_L(\hat{\mathbf{r}}) [\phi^a_{i_1}(\mathbf{r}) \phi^a_{i_2}(\mathbf{r}) - \tilde{\phi}^a_{i_1}(\mathbf{r}) \tilde{\phi}^a_{i_2}(\mathbf{r})] \end{aligned} \tag{3.44}$$

3.4.4 Summary

By summing up all the terms we derived above, we finally obtain the sought separation of the total energy into the smooth and atom-centered contributions

$$E = \tilde{E} + \sum_a (E^a - \tilde{E}^a) \tag{3.45}$$

where

$$\tilde{E} = \tilde{T}_s + U[\tilde{\rho}] + E_{xc}[\tilde{n}] \tag{3.46}$$

$$E^a = \sum_a (T_s^a + U[\rho^a] + E_{xc}[n^a]) \tag{3.47}$$

$$\tilde{E}^a = \sum_a (\tilde{T_s}^a + U[\tilde{\rho}^a] + E_{xc}[\tilde{n}^a]) \tag{3.48}$$

By using (3.41) and (3.43), the atom-centered correction $E^a - \tilde{E}^a$ can be written as a function of the density matrix $D^a_{i_1 i_2}$

$$\begin{aligned} E^a - \tilde{E}^a &= \Delta E^a[\{D^a_{i_1 i_2}\}] \\ &= A^a + \sum_{i_1 i_2} B^a_{i_1 i_2} D^a_{i_1 i_2} + \sum_{i_1 i_2 i_3 i_4} D^{a*}_{i_1 i_2} C^a_{i_1 i_2 i_3 i_4} D^a_{i_3 i_4} + \Delta E_{xc}(\{D^a_{i_1 i_2}\}) \end{aligned} \tag{3.49}$$

where A^a, $B^a_{i_1 i_2}$ and $C^a_{i_1 i_2 i_3 i_4}$ are system-independent tensors which can be pre-calculated and stored for each relevant chemical element.

3.5 Transformed Kohn-Sham equations

The PAW variational parameters are the pseudo wavefunctions $\{\psi_n\}$. These can be obtained either by solving the all-electron Kohn-Sham equations and subsequently transforming the resulting wavefunctions, or by solving the transformed Kohn-Sham equations

$$\tilde{\hat{H}} \, |\tilde{\psi}_n\rangle = \epsilon_n \hat{S} \, |\tilde{\psi}_n\rangle \tag{3.50}$$

where $\hat{S} = \hat{\mathcal{T}}^\dagger \hat{\mathcal{T}}$ is the overlap operator and $\tilde{\hat{H}} = \hat{\mathcal{T}}^\dagger \hat{H} \hat{\mathcal{T}}$ is the transformed Hamiltonian.

3.5.1 Overlap operator

The PAW overlap operator can be obtained directly by transforming the unity operator according to (3.17)

$$\begin{aligned} \hat{S} = \hat{\mathcal{T}}^\dagger \hat{1} \hat{\mathcal{T}} &= 1 + \sum_a \sum_{i_1, i_2} |\tilde{p}^a_{i_1}\rangle \left(\langle \phi^a_{i_1} | \tilde{\phi}^a_{i_2} \rangle - \langle \tilde{\phi}^a_{i_1} | \phi^a_{i_2} \rangle \right) \langle \tilde{p}^a_{i_2}| \\ &= 1 + \sum_a \sum_{i_1, i_2} |\tilde{p}^a_{i_1}\rangle \sqrt{(4\pi)} \Delta^a_{00,ij} \langle \tilde{p}^a_{i_2}| \end{aligned} \tag{3.51}$$

The orthogonality condition for the eigenstates of the Kohn-Sham equations then becomes

$$\langle \psi_n | \psi_m \rangle = \delta_{nm} \quad \Rightarrow \quad \langle \tilde{\psi}_n | \hat{S} | \tilde{\psi}_m \rangle = \delta_{nm} \tag{3.52}$$

i.e. the pseudo wavefunctions are orthogonal with respect to the weight $\hat{S}$.

3.5.2 Hamiltonian operator

In order to write the transformed Hamiltonian as the usual sum of the smooth and the atom-centered contributions, we use the fact that

$$\frac{\delta E}{\delta \tilde{\psi}^*_n} = f_n \tilde{\hat{H}} \tilde{\psi}_n \tag{3.53}$$

to explicitly calculate the derivative of the total energy (3.45)

$$\begin{aligned}
\frac{\delta E}{\delta \tilde{\psi}_n^*(\mathbf{r})} &= \frac{\delta}{\tilde{\psi}_n^*(\mathbf{r})}\left[T[\tilde{\psi}_n^*] + U[\tilde{\rho}] + E_{xc}[\tilde{n}]\Delta E^a[\{D^a_{i_1 i_2}\}]\right] \\
&= \frac{\delta T[\{\tilde{\psi}_n^a\}]}{\delta \tilde{\psi}_n^*} + \int d\mathbf{r}' \left[\frac{\delta E_{xc}[\tilde{n}]}{\delta \tilde{n}(\mathbf{r}')} + \frac{\delta U[\tilde{\rho}]}{\delta \tilde{n}(\mathbf{r}')}\right]\frac{\delta \tilde{n}(\mathbf{r}')}{\delta \tilde{\psi}_n^*(\mathbf{r})} + \\
&+ \sum_a \sum_{i_1 i_2}\left[\int d\mathbf{r}' \frac{\delta U_H[\tilde{n} + \sum_a \tilde{Z}^a]}{\delta Z^a(\mathbf{r}')}\frac{\delta Z^a(\mathbf{r}')}{\delta D^a_{i_1 i_2}} + \frac{\delta \Delta E^a}{\delta D^a_{i_1 i_2}}\right]\frac{\delta D^a_{i_1 i_2}}{\delta \tilde{\psi}_n^*(\mathbf{r})} \\
&= -\frac{1}{2}\nabla^2 f_n \tilde{\psi}_n(\mathbf{r}) + \int d\mathbf{r}' \left[v_{xc}[\tilde{n}](\mathbf{r}') + u_H[\tilde{\rho}](\mathbf{r}')\right] f_n \delta(\mathbf{r} - \mathbf{r}')\tilde{\psi}_n(\mathbf{r}') + \\
&+ \sum_a \sum_{i_1 i_2}\left[\int d\mathbf{r}' u_H[\tilde{n} + \sum_a \tilde{Z}^a](\mathbf{r}') \sum_L \Delta^a_{L i_1 i_2}\tilde{g}^a_L(\mathbf{r}') + \frac{\delta \Delta E^a}{\delta D^a_{i_1 i_2}}\right] f_n \tilde{p}^a_{i_1}(\mathbf{r}) P^a_{n i_2}
\end{aligned} \tag{3.54}$$

Using (3.53) we then obtain the transformed Hamiltonian as

$$\tilde{\hat{H}} = -\frac{1}{2}\nabla^2 + u_H[\tilde{\rho}] + v_{xc}[\tilde{n}] + \sum_a \sum_{i_1 i_2} |\tilde{p}^a_{i_1}\rangle \, \Delta H^a_{i_1 i_2} \, \langle \tilde{p}^a_{i_2}| \tag{3.55}$$

where the atomic corrections $\Delta H^a_{i_1 i_2}$ are given as the tensor

$$\begin{aligned}
\Delta H^a_{i_1 i_2} &= \sum_L \Delta^a_{L i_1 i_2} \int d\mathbf{r} u_H[\tilde{\rho}]\tilde{g}^a_L(\mathbf{r}) + \frac{\delta \Delta E^a}{\delta D^a_{i_1 i_2}} \\
&= \sum_L \Delta^a_{L i_1 i_2} \int d\mathbf{r} u_H[\tilde{\rho}]\tilde{g}^a_L(\mathbf{r}) + B^a_{i_1 i_2} + 2\sum_{i_3 i_4} C^a_{i_1 i_2 i_3 i_4} D^a_{i_3 i_4} + \frac{\delta \Delta E^a}{\delta D^a_{i_1 i_2}}
\end{aligned} \tag{3.56}$$

Chapter 4

Implementations

In order to solve the Kohn-Sham equations (3.2), the wavefunction needs to be evaluated. For this, one can use real-space grids to directly sample the values of the wavefunction at the grid points or one can expand the wavefunction in some basis-set.

This chapter will review the most important aspects of different standard computational approaches to the calculation of single-particle states of a Schrödinger-like equation.

4.1 Boundary conditions

Like any other differential equations, the Kohn-Sham equations must be solved subjected to appropriate boundary conditions (BCs).

4.1.1 Periodic systems

Solving the Schrödinger equation, or equivalently the K-S equations, for an infinite periodic system is in principle impossible, as it requires solving for an infinite number of states over an infinite domain. Fortunately the form of these equations provides a general property which simplifies the problem in the case of periodic potentials

Bloch's theorem 4.1.1 *The eigenstates of the single particle Hamiltonian* $H = \frac{-\hbar\nabla^2}{2m} + V(\mathbf{r})$*, where* $V(\mathbf{r}) = V(\mathbf{r}+\mathbf{R})$ *for all* $\mathbf{R}$ *in a Bravais lattice, can be chosen to have the form*

$$\psi_{n\mathbf{k}}(\mathbf{r}) = e^{i\mathbf{k}\cdot\mathbf{r}} u_{n\mathbf{k}}(\mathbf{r}), \tag{4.1}$$

i.e. as plane waves times a function with the periodicity of the lattice. An equivalent form is

$$\psi_{n\mathbf{k}}(\mathbf{r}+\mathbf{R}) = e^{i\mathbf{k}\cdot\mathbf{r}} \psi(\mathbf{r}). \tag{4.2}$$

As a consequence, the wave vector $\mathbf{k}$ of a Bloch state can always be confined to the first Brillouin zone, because if $\mathbf{k}'$ lies outside then $\mathbf{k}' = \mathbf{k} + \mathbf{K}$ and $e^{i\mathbf{K}\cdot\mathbf{R}} = 1$. The allowed values of $\mathbf{k}$ are then dictated by the boundary conditions.

Bloch's representation points out that the number of occupied states is finite, at each k-point, even for infinite periodic systems. This transforms the problem of computing an infinite number of wave functions into the problem of computing a finite number, for an infinite number of k-points. By also noting that states with similar $\mathbf{k}$ vector are similar, this provides a practical way to convert integrals over all space into averages on values sampled at an appropriate set of k-points only inside the first Brilluoin zone.

In real-space grids approaches one directly enforces (4.2) at the unit-cell boundaries. This means that one has then to solve the Kohn-Sham equations with different BCs for each $\mathbf{k}$ but the Hamiltonian remains unaffected by the periodicity, and thus fixed.

In plane-wave implementations periodic boundary conditions arise in a natural way, as they form a basis expansion for $u_{n\mathbf{k}}(\mathbf{r})$. Differently from the real-space case, here the Hamiltonian $\hat{H} = \hat{H}(\mathbf{k})$ is different for each $\mathbf{k}$, but the BCs are then the same for each $\mathbf{k}$.

4.1.2 Finite systems

In order to describe finite non-periodic systems, Dirichlet (or vanishing) boundary conditions are the appropriate choice

$$\psi_n(\mathbf{r}) = 0 \quad \text{for } \mathbf{r} \text{ outside the unit cell} \tag{4.3}$$

Enforcing Dirichlet boundary conditions is straightforward in real-space grids and localized basis-sets approaches.

However, by using super-cells, it is also possible to treat finite systems using periodic boundary conditions. This is for instance necessary for plane-wave bases, since they *per se* require periodicity. This is achieved by including enough vacuum around the system under investigation, so that the interaction between neighboring cells goes to zero. The so-called supercell approach consists in infinitely repeating the unit cell in the directions which are to be treated with periodic conditions. In this way a superlattice is produced, and Bloch theorem applies.

4.2 Basis-Sets

Any element of a vector space can be expressed as a linear combination of base vectors. In quantum mechanics, a quantum state (-vector) is an element of an infinite-dimensional Hilbert space. In principle, given a state $|\psi_n\rangle$, an infinite number of basis functions is required in order to reproduce

it. The basis-set $\{\Phi\}$ is termed complete if any element of the space can be written as a linear combination of base vectors.

$$\psi_n = \sum_\mu c_{n\mu}\Phi_\mu \tag{4.4}$$

The solution to the Kohn-Sham equation can be found by expanding the wavefunctions onto a truncated basis set, in order to obtain a finite matrix eigenvalue problem. The main issue is, of course, the choice of a "good" basis set. The accuracy of the approximation will be high if the basis-set approaches the complete basis limit.

4.2.1 Plane waves

Since $u_{n\mathbf{k}}(\mathbf{r})$ is cell-periodic, it can be expressed as a discrete Fourier sum. Equation (4.1) then reads

$$\psi_{n\mathbf{k}} = \sum_{\mathbf{G}} c_{n\mathbf{k}} e^{i(\mathbf{k}+\mathbf{G})\cdot\mathbf{r}}, \tag{4.5}$$

where $\mathbf{G}$ is any reciprocal lattice vectors and the normalization factor $1/V$ over the volume of the supercell has been absorbed into the expansion coefficients. By inserting (4.5) into the Kohn-Sham equations we find the matrix eigenvalue problem

$$\sum_{\mathbf{G}'} \left[\frac{1}{2}|\mathbf{k}+\mathbf{G}'|^2\delta_{\mathbf{G}\mathbf{G}'} + V^{\text{eff}}_{\mathbf{G}-\mathbf{G}'}\right] c_{n\mathbf{k}+\mathbf{G}'} = \epsilon_n c_{n\mathbf{k}+\mathbf{G}}, \tag{4.6}$$

where $V^{\text{eff}}_{\mathbf{G}-\mathbf{G}'}$ are the Fourier coefficient of V^{eff}.

Although Bloch theorem reduced the continuous plane-wave expansion to a discrete sum, the sums over the reciprocal lattice vector are still infinite. In order to obtain a finite matrix problem, the expansion must be truncated. This is achieved by introducing a cut-off energy E_{cut} for the plane waves, such that only plane waves that satisfy $\frac{1}{2}|\mathbf{k}+\mathbf{G}|^2 \leq E_{cut}$ are included in the expansion (4.5).

The main advantages of a plane-wave basis are:

1. The convergence of the result can then be controlled just by one parameter, i.e. E_{cut}.

2. Plane waves are orthonormal and independent of the atomic positions, i.e. there is no basis-set superposition error and Pulay forces.

3. Integrals and derivatives can be efficiently computed in reciprocal space, making it easy to calculate the matrix elements of the Hamiltonian.

On the other hand, the computational cost of a well-converged calculation is usually high, especially for isolated systems, where the required number of plane waves is large. Plane waves, in fact, cannot take advantage of the vacuum to reduce the size of the basis. In order to conveniently reduce E_{cut}, smooth pseudopotentials must be employed. Furthermore efficient parallelization is problematic due to the mathematics of delocalized plane waves. The required Fourier transforms are actually very difficult to parallelize.

4.2.2 Analytical atomic orbitals

Gaussian orbitals

Gaussian-type orbitals (GTO) are the most widely used basis-set used in quantum-chemical wavefunction methods.

$$\psi(\mathbf{r}) = x^i y^j z^k e^{-\alpha r^2} Y_{lm}(\theta, \phi), \tag{4.7}$$

where α is an orbital-dependent parameter setting the width of the function, and $l = i + j + k$ is used to classify the GTO as $s-$type ($l = 0$), $p-$type ($l = 1$), etc. Their form is not suggested by physical arguments, but because they are numerically easy to deal with. By taking advantage of the fact that the product of gaussians is still a gaussian, many-center integrals can be computed analytically using very efficient schemes.

Since a GTO alone does not resemble a real atomic eigenfunction, one can then contract several of them together in a fixed linear combination to give a Contracted Gaussian function (CGF). The expansion coefficient are chosen in such a way that the CGF resembles as much as possible a single STO (see below). In this way the number of basis functions can be reduced, still mantaining the computational advantages of gaussian functions.

Slater-type orbitals

Slater-type orbitals (STO) were the first basis set used in quantum chemistry, suggested by the form of the analytical solution for the isolated hydrogen atom

$$\psi(\mathbf{r}) = r^{n-1} e^{-\zeta r} Y_{lm}(\theta, \phi), \tag{4.8}$$

where ζ is an orbital exponent and n is the principal quantum number. As $r \to 0$ these orbitals exhibit the correct cusp behavior (while GTOs go to zero with zero slope) and the exponential decay as $r \to \infty$ (while GTOs fall off too quickly). For this reason one needs fewer STOs than GTOs in order to achieve a given accuracy. On the other hand, many-center integrals are much more difficult to compute with STOs, since some work cannot be done analytically.

4.2.3 Numerical atomic orbitals

Numerical atomic orbitals are obtained as solutions of the radial Kohn-Sham equation for a given isolated atom times spherical harmonics

$$\psi_i(\mathbf{r}) = \varphi_i(r)Y_{lm}(\hat{\mathbf{r}}). \tag{4.9}$$

These orbitals are represented numerically by means of spline interpolation between grid points. The physical origin of such orbitals, i.e. that they are exact for atoms within the given xc-functional, allows one to use a small basis-set size and still get reasonable accuracy.

4.2.4 Basis Set Superposition Error

Let us assume that we have some atom-centered basis set, which move along with the atoms in the system. Then, if we have a system of interacting constituents described by incomplete basis-sets, each constituent will lower its energy by taking advantage of part of the other constituent's basis. This will of course introduce an unphysical effect in the calculation of interaction energies due to the better description of the constituents when they are interacting (in a complex) than when they are isolated.

The most widely used method to handle this Basis Set Superposition Error (BSSE) has been the "Counterpoise" method of Boys and Bernardi [7]. This consists in providing the isolated constituents with the full basis they would have in the interacting complex. For instance, if we have a complex AB made up of two interacting constituents A and B, the Counterpoise-corrected interaction energy is

$$\Delta E(AB) = A(AB, r_p)^{AB} - E(A, r_c)^{AB} - E(B, r_c)^{AB}, \tag{4.10}$$

where r_p indicates the geometry of the product AB, r_c the geometry of the constituents and the superscript AB indicates that the energies are calculated with the same basis, i.e. the basis of the product.

4.3 Real-Space and Finite-Differences

With the real-space finite-difference method, the wavefunctions, density and potential are directly calculated on a grid, instead of using basis functions. Differentiation is the major basic operation we need in order to discretize the Kohn-Sham equations. The $k-$th order derivative of a function $f(x)$ at a grid point $x = ih_x$ is approximated by the finite-difference formula

$$\frac{d^{(k)}}{dx^{(k)}} f(x)\Big|_{x=ih_x} \approx \sum_{n=-N_f}^{N_f} c_n^{(k)} f(ih_x + nh_x), \tag{4.11}$$

where N_f sets the accuracy of the finite-difference approximation and h_x is the grid spacing along the x direction. The weights $c_n^{(k)}$ are determined using the Taylor expansion.

The one-dimensional Kohn-Sham equation discretized in real space is thus given by

$$-\frac{1}{2}\sum_{n=-N_f}^{N_f} c_n^{(2)}\psi(ih_x + nh_x) + V^{eff}(ih_x)\psi(ih_x) = \epsilon\psi(ih_x). \tag{4.12}$$

As for plane-wave approaches, the desired accuracy can be increased in a simple definite manner, which consists in reducing the grid-spacing and improving the order of the finite-difference approximations.

Although finite-difference methods have been very common in scientific applications for decades, they have been gaining focus only recently in first-principle calculations. This means that one can take advantages of highly developed and optimized techniques, such as multi-grid methods [9]. Efficient parallelization by domain decomposition is easily achieved, enabling the use of massively parallel supercomputers [25]. Furthermore, since arbitrary boundary conditions are available in real space, this approach can reproduce the conditions of an actual experiment.

We finally note that, since all calculations are carried out in real-space, it is possible to incorporate a local basis set within the same implementation.

Chapter 5

LCAO in PAW

Most of the available implementations of the PAW method use a plane-wave basis set to expand the pseudo wavefunction $\tilde{\psi}_n$ [28, 23, 16]. The GPAW code [1] implements a real-space approach, by evaluating $\tilde{\psi}_n$ on a grid and using finite-difference methods. These approaches have proven very useful and they compare well to pseudopotential results in most cases [23]. Nevertheless PAW methods perform significantly better for evaluation of magnetic energies [23]. They also compare remarkably well to all-electron calculations of electric field gradients [31], magnetic hyperfine parameters [6] and NMR chemical shifts [32].

In this chapter we will expand the pseudo-wavefunction $\tilde{\psi}_n$ onto a local basis-set, constructed as a linear combination of atom-centered functions which we will abbreviate "LCAO"[1].

Numerical local orbitals have been previously employed in DFT, using either all-electron [27, 20] or pseudopotential methods [18]. There are at least two relevant areas where this approach has proven very useful:

1. very large systems with many atoms per unit-cell or with vacuum regions, where plane-waves becomes expensive to use [3] [35];

2. combination with Green's functions-type methods, that take direct advantage of the locality of the basis [8].

To my knowledge this is the first implementation of a localized basis in the Projector Augmented Wave method. It should be stressed that the two different "modes", i.e. grid and localized basis, share exactly the same set of approximations, which is also a unique feature.

[1] Linear Combination of Atomic Orbitals. Strictly speaking, we use atomic-*like* functions.

5.1 LCAO basis-sets

We use atom-centered orbitals that are the products of numerical radial functions and spherical harmonics

$$\Phi_{nlm}(\mathbf{r}) = \varphi_{nl}(r^a)Y_{lm}(\hat{\mathbf{r}}^a), \tag{5.1}$$

where $r^a = \mathbf{r} - \mathbf{R}^a$ is the position of nucleus a.

The Kohn-Sham wavefunction is then expressed as the expansion

$$\psi_n = \sum_N c_{\mu n}\Phi_\mu, \tag{5.2}$$

where $\mu = (n, l, m)$ is a combined quantum label.

5.1.1 Naming conventions

By following the well-established notation of the quantum chemistry community, we classify the basis-set according to the number of basis functions which are used for each atomic element. If only one radial function φ_{nl} for each occupied valence[2] orbital $|nl\rangle$ is used, we have what is known as a "Single-Zeta" (SZ) basis-set, also known as a "minimal" basis. For example, a SZ basis for hydrogen contains just one $s-$type function.

Multiple-Zeta sets are obtained by generating multiple functions for each valence state of the given atom. For example a Double-Zeta (DZ) basis set for H consists of 2 $s-$type functions, while for O it consists of 2 $s-$type plus 2×3 $p-$type functions, i.e. 8 basis functions. Multiple-Zeta orbitals are generated in such a way as to improve the radial flexibility of the basis-set.

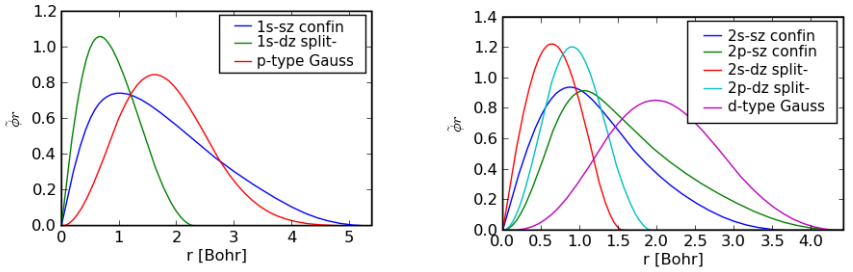

(a) **(b)**

Figure 5.1: *DZP basis for H (a) and O (b)*

In order to improve the angular flexibility, higher angular momentum l functions, termed "polarization" functions, are added to the set, making it

[2] in contrast with quantum-chemical all-electron methods, where basis functions for core states are also needed.

a polarized basis-set. This is usually achieved by adding a function with angular momentum $l+1$ where l is the highest occupied valence orbital of the isolated atom. If only one polarization function is added on top of a single-zeta basis, we have what is known as "Single-Zeta Polarized" (SZP) basis. Similarly we can obtain double-zeta polarized (DZP) or even larger basis-sets. As an example, a DZP basis for O consists of 8 functions from the DZ part, plus a $d-$type orbital ($m=-2,-1,0,+1,+2$) which gives 13 functions in total. Multiple-polarized basis sets can also be constructed.

5.1.2 Generation

In order to take advantage of the sparsity of the Hamiltonian and Overlap matrices in the basis-set representation, we use strictly localized basis orbitals, i.e orbitals that are identically zero beyond a given radius. As proposed by Sankey and Niklewski [34, 33], and successfully implemented in the SIESTA method [18], we take the SZ basis orbitals φ_{nl} to be the pseudo-eigenfunctions of the isolated atom confined in some spherical potential well $V^{conf}(r)$

$$\left(-\frac{1}{2r}\frac{d^2}{dr^2}r+\frac{l(l+1)}{2r^2}+V^{eff}(r)+V^{conf}(r)\right)\varphi_{nl}=\varepsilon_{nl}\varphi_{nl}. \tag{5.3}$$

The confinement potential is constructed so that it is constant in the core region, starts off at some radius r_i with all derivatives continuous, and diverges at r_c, so that any orbital is strictly localized. The explicit form is [19]

$$V^{conf}(r)=V_0\frac{e^{-(r_c-r_i)/(r-r_i)}}{r_c-r}. \tag{5.4}$$

An infinite spherical well, as originally proposed in [34], would involve just one parameter r_c (instead of three r_c, r_i, V_o) but would generate basis orbitals with derivative discontinuity for $r=r_c$. This kink might cause numerical problems when differentiated wavefunctions are needed, for instance in a force calculation. As it is natural for different orbitals to have different cut-off radii r_c, we define a common energy-shift $\delta\varepsilon_{nl}$

$$\delta\varepsilon_{nl}=\varepsilon_{nl}\Big|_{V^{conf}\neq 0}-\varepsilon_{nl}\Big|_{V^{conf}=0}, \tag{5.5}$$

i.e. the shift in the corresponding eigenvalue when the confining potential is switched on. The cut-off radius is then found by specifying $\delta\varepsilon_{nl}$ and requiring that (5.3) is fulfilled with $\varepsilon_{nl}+\delta\varepsilon_{nl}$ as eigenvalue. In practice, we use a common energy shift for all orbitals, denoted by ΔE.

As for multiple-zetas, we use the standard quantum chemical "split-valence method" adapted to numerical orbitals [12]. According to this procedure, the DZ function is obtained by mantaining the same tail as the SZ,

but changing to a 2^{nd} order polynomial inside some split-radius r_s^{nl}:

$$\varepsilon_{nl}^{DZ}(r) = \begin{cases} r^l(a_{nl} - b_{nl}r^2) & \text{if } r < r_s^{nl} \\ \varphi_{nl}^{SZ}(r) & \text{if } r \geq r_s^{nl} \end{cases} \tag{5.6}$$

where a_{nl} and b_{nl} are determined to ensure continuity of value and derivative at r_s^{nl}. The split-radius r_s^{nl} is determined by specifying the "tail-norm", i.e the value of $\int_{r_s^{nl}}^{r_c^{nl}} \varphi_{nl}^{SZ} dr^3$. In practice, in order to get shorter ranged basis functions, we use $\varphi_{nl}^{SZ} - \varphi_{nl}^{DZ}$ as second-zeta orbital.

The basis orbitals described so far are all-electron functions. Since they should be used to expand the pseudo-wavefunctions $\tilde{\psi}_n$, we need to apply the PAW transformation so that we obtain the pseudo basis functions:

$$|\tilde{\varphi}_{nl}^{mZ}\rangle = \hat{\mathcal{T}}^{-1} |\varphi_{nl}^{mZ}\rangle \,, \tag{5.7}$$

where the superscript mZ denotes a generic Multiple-Zeta basis.

Polarization functions are taken to be simple pseudo-gaussian with a given width r_{char}^l

$$\varphi_{nl}^{P}(r) = r^{l+1} e^{-(\frac{r}{r_{char}^l})^2}. \tag{5.8}$$

This simple approach has proven very satisfactory despite its simplicity. Indeed it compares really well to more sophisticated methods, such as perturbation of the isolated atom by electric fields as done in SIESTA.

In order to optimize a basis set, the free parameters r_i, V_0, r_s and r_{char} can be variationally optimized for some reference systems. A more detailed and comprehensive description about the generation of basis functions can be found in Ask Hjorth Larsen's master thesis.

5.1.3 Bloch states

In order to fulfill the Bloch condition (4.1)-(4.2) with a local basis-set, we seek solutions of the Kohn-Sham problem which resemble the Tight-Binding problem

$$\tilde{\psi}_{n\mathbf{k}}(\mathbf{r}) = \sum_{\mathbf{R}} e^{i\mathbf{k}\cdot\mathbf{R}} \tilde{\psi}_n(\mathbf{r} - \mathbf{R}), \tag{5.9}$$

where $\mathbf{R}$ spans all the Bravais lattice and $\mathbf{k}$ takes the values allowed by the periodic boundary conditions only within the first Brillouin zone.

By plugging the expansion (5.2) into (5.9) we get

$$\psi_{n\mathbf{k}}(\mathbf{r}) = \sum_{\mu\mathbf{R}} c_{\mu n\mathbf{k}} \Phi_\mu(\mathbf{r}) e^{i\mathbf{k}\cdot\mathbf{R}}, \tag{5.10}$$

[3] Strictly speaking, this is not a norm, but rather a "tail-area" since the integrand is not squared.

i.e. the wavefunctions become complex and k-dependent. Note that this is equivalent to consider the unit-cell being reproduced in space. Each contribution from a different phase factor then corresponds to a contribution from a neighboring cell (Fig. 5.2). In practice we add supplementary cells as far

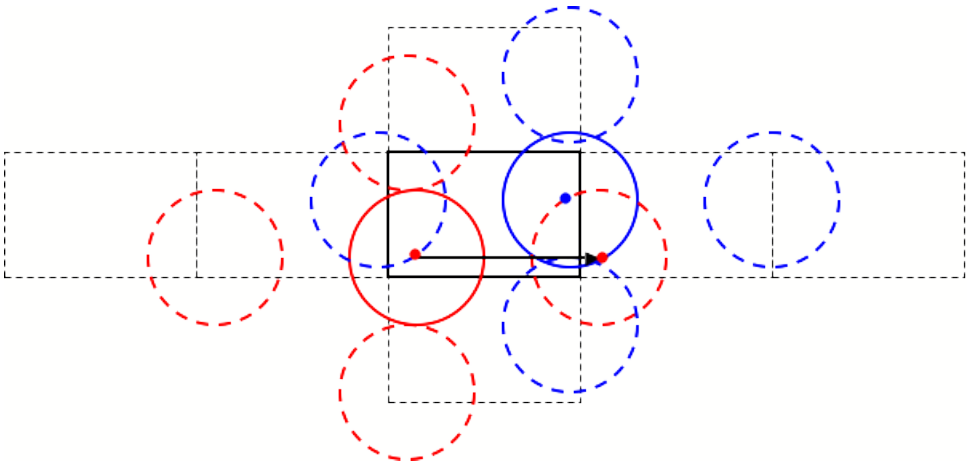

Figure 5.2: *Unit cell and neighbouring mirror-cells.*

as their basis orbitals have non-zero overlap with the unit-cell.

5.2 Kohn-Sham equations in the LCAO basis

The variational freedom in the Kohn-Sham minimization procedure is drastically reduced by employing a basis-set, because the Kohn-Sham equation is to be solved for each expansion coefficient $c_{\mu n}$ in (5.2) instead of at each grid point. By inserting (5.2) in the PAW Kohn-Sham equation we obtain the matrix equation

$$\tilde{\hat{H}}C = \epsilon \hat{S}C, \tag{5.11}$$

where the eigenvectors C contain the coefficients $\{c_{\mu n}\}$. The PAW Hamiltonian is, as derived in Chapter 2,

$$\tilde{\hat{H}} = -\frac{1}{2}\nabla^2 + u_H[\tilde{\rho}] + v_{xc}[\tilde{n}] + \sum_a \sum_{i_1 i_2} |\tilde{p}^a_{i_1}\rangle \, \Delta H^a_{i_1 i_2} \, \langle \tilde{p}^a_{i_2}| \, . \tag{5.12}$$

The matrix elements of the first and last terms involve only two-center integrals, which we calculate analytically in the reciprocal space and tabulate as a function of the distance vector. Since densities and potentials are calculated on a grid, the remaining terms must be integrated numerically.

5.2.1 Overlap operator

Since we use a non-orthogonal basis, the matrix elements of the Kohn-Sham wavefunctions with the PAW overlap operator $\langle\tilde{\psi}_{i\mathbf{k}}|\hat{S}|\tilde{\psi}_{j\mathbf{k}}\rangle$ acquire some basis-specific overlap contributions. Since Bloch states belonging to different k-points are orthogonal, and since the PAW overlap operator does not couple different k-points, we just need to consider matrix elements between states at the same k-point.

By expanding the wavefunction onto the Bloch basis (5.10) and inserting it into the expression for the PAW overlap operator (3.51), we obtain

$$\begin{aligned}\langle\tilde{\psi}_{i\mathbf{k}}|\,\hat{S}\,|\tilde{\psi}_{j\mathbf{k}}\rangle = \sum_{\mu,\mathbf{R}}\sum_{\nu,\mathbf{R}'} c^*_{\mu i\mathbf{k}}c_{\nu j\mathbf{k}}\,\langle\tilde{\Phi}_{\mu\mathbf{R}}|\tilde{\Phi}_{\nu\mathbf{R}'}\rangle\,e^{i\mathbf{k}\cdot(\mathbf{R}'-\mathbf{R})}+\\ +\sum_{\mu,\nu}\sum_{a,\mathbf{Q}}\sum_{\mathbf{R},\mathbf{R}'}\sum_{i_1,i_2} c^*_{\mu i\mathbf{k}}c_{\nu j\mathbf{k}}\,\langle\tilde{\Phi}_{\mu\mathbf{R}}|\tilde{p}^{a,\mathbf{Q}}_{i_1}\rangle\,\Delta S^a_{i_1i_2}\,\langle\tilde{p}^{a,\mathbf{Q}}_{i_2}|\tilde{\Phi}_{\nu\mathbf{R}'}\rangle\,e^{i\mathbf{k}\cdot(\mathbf{R}'-\mathbf{R})},\end{aligned} \tag{5.13}$$

where R, R' refers to cells where basis functions are located and $\mathbf{Q}$ is the cell where the projector of atom a is located. Rearranging the terms and noting that the inner products depend only on the relative position of the centers, we obtain the final expression for the overlap between state $|i\rangle$ and $|j\rangle$

$$\begin{aligned}\langle\tilde{\psi}_{i\mathbf{k}}|\,\hat{S}\,|\tilde{\psi}_{j\mathbf{k}}\rangle = \sum_{\mu,\nu} c^*_{\mu i\mathbf{k}}c_{\nu j\mathbf{k}}\sum_{\bar{\mathbf{R}}}\langle\tilde{\Phi}_{\mu\mathbf{0}}|\tilde{\Phi}_{\nu\bar{\mathbf{R}}}\rangle\,e^{i\mathbf{k}\cdot\bar{\mathbf{R}}}+\\ +\sum_{\mu,\nu} c^*_{\mu i\mathbf{k}}c_{\nu j\mathbf{k}}\sum_{a,i_1,i_2}\Delta S^a_{i_1i_2}\left(\sum_{\mathbf{R}}\langle\tilde{\Phi}_{\mu\mathbf{R}}|\tilde{p}^{a,\mathbf{0}}_{i_1}\rangle\,e^{i\mathbf{k}\cdot\mathbf{R}}\right)\left(\sum_{\mathbf{R}'}\langle\tilde{p}^{a,\mathbf{0}}_{i_2}|\tilde{\Phi}_{\nu\mathbf{R}'}\rangle\,e^{i\mathbf{k}\cdot\mathbf{R}'}\right),\end{aligned} \tag{5.14}$$

where $\bar{\mathbf{R}} = \mathbf{R}' - \mathbf{R}$.

Note that in expression (5.14) we can recognise the usual PAW form, that is to say a first delocalized term plus the atomic corrections inside the augmentation spheres.

5.2.2 Hamiltonian operator

The Hamiltonian contains the same types of terms as the overlap operator. It is derived by expanding the wavefunction onto the basis-set (5.2) and plugging it into the expression for the PAW Hamiltonian operator (5.12).

We then obtain

$$\begin{aligned}\langle\psi_{i\mathbf{k}}|\,\hat{H}\,|\psi_{j\mathbf{k}}\rangle &= \sum_{\mu,\nu} c^*_{\mu i\mathbf{k}} c_{\nu j\mathbf{k}} \sum_{\bar{\mathbf{R}}} \langle\phi_{\mu\mathbf{0}}|\hat{T}|\phi_{\nu\bar{\mathbf{R}}}\rangle\, e^{i\mathbf{k}\cdot\bar{\mathbf{R}}} + \\ &+ \sum_{\mu,\nu} c^*_{\mu i\mathbf{k}} c_{\nu j\mathbf{k}} \sum_{\bar{\mathbf{R}}} \langle\phi_{\mu\mathbf{0}}|\hat{V}_{eff}|\phi_{\nu\bar{\mathbf{R}}}\rangle\, e^{i\mathbf{k}\cdot\bar{\mathbf{R}}} + \\ &+ \sum_{\mu,\nu} c^*_{\mu i\mathbf{k}} c_{\nu j\mathbf{k}} \sum_{a,i_1,i_2} \Delta H^a_{i_1 i_2} \left(\sum_{\mathbf{R}} \langle\phi_{\mu\mathbf{R}}|\tilde{p}^{a,\mathbf{0}}_{i_1}\rangle\, e^{i\mathbf{k}\cdot\mathbf{R}}\right)\left(\sum_{\mathbf{R}'} \langle\tilde{p}^{a,\mathbf{0}}_{i_2}|\phi_{\nu\mathbf{R}'}\rangle\, e^{i\mathbf{k}\cdot\mathbf{R}'}\right).\end{aligned} \tag{5.15}$$

As we see from (5.15), the main ingredients are the matrix elements of the kinetic operator and the inner products between basis functions and projectors. The following section describes how they can be calculated analytically.

5.3 Two-center integrals

All the two center integrals which do not involve potentials on the grid are calculated analytically in Fourier space, following [34, 18]. Let us consider a general overlap integral

$$\Theta(\mathbf{R}) = \langle\mathcal{X}_1|\mathcal{X}_2\rangle = \int \mathcal{X}^*_1(\mathbf{r})\mathcal{X}_2(\mathbf{r}-\mathbf{R})dr, \tag{5.16}$$

where the integral is over all space and $\mathcal{X}_i$ are localized functions which can be expressed as a product of a radial function times a spherical harmonic

$$\begin{aligned}\mathcal{X}(\mathbf{r}) &= \chi_l(r)Y_{lm}(\hat{r}) \\ \chi_l(r) &= \int_0^{\pi} \sin\theta d\theta \int_0^{2\pi} d\varphi Y^*_{lm}(\theta,\varphi)\mathcal{X}(r,\theta,\varphi).\end{aligned} \tag{5.17}$$

By noting that $\Theta(\mathbf{R})$ can be seen as a convolution, we write it as a product in the Fourier space

$$\Theta(\mathbf{R}) = \int \mathcal{X}^*_1(\mathbf{k})\mathcal{X}_2(\mathbf{k})e^{-ik\mathbf{R}}d\mathbf{r}, \tag{5.18}$$

where

$$\mathcal{X}(\mathbf{k}) = \frac{1}{(2\pi)^{(3/2)}} \int \mathcal{X}(\mathbf{r})e^{-ik\mathbf{r}}d\mathbf{r}. \tag{5.19}$$

Let us expand a plane wave in spherical harmonics

$$e^{ikr} = \sum_{l=0}^{\infty}\sum_{m=-l}^{l} 4\pi i^l j_l(kr)Y^*_{lm}(\hat{k})Y_{lm}(\hat{r}) \tag{5.20}$$

where $j_l(kr)$ is a l^{th} order spherical Bessel function and insert it into (5.19) to obtain

$$\mathcal{X}(\mathbf{k}) = \chi_l(k) Y_{lm}(\hat{k}) \tag{5.21}$$

$$\chi_l(k) = \sqrt{\frac{2}{\pi}}(-i)^l \int_0^\infty r^2 j_l(kr) \mathcal{X}_l(r) dr \tag{5.22}$$

Finally, by substituting (5.21) and (5.22) into (5.18) we obtain

$$\Theta(\mathbf{R}) = \sum_{l=0}^{\infty} \sum_{m=-l}^{l} \Theta_{lm}(R) Y_{lm}(\hat{R}), \tag{5.23}$$

where

$$\Theta_{lm} = G_{l_1 m_1, l_2 m_2, lm} \Theta_{l_1, l_2, l}(R) \tag{5.24}$$

$$\Theta_{l_1,l_2,l} = 4\pi i^{l_1 - l_2 - l} \int k^2 j_l(kR) i^{-l_1} \chi^*_{1,l_1}(k) i^{l_2} \chi_{2,l_2}(k) dk. \tag{5.25}$$

The Gaunt coefficients $G_{l_1 m_1, l_2 m_2, lm}$ are non-zero only if $l_1 - l_2 - l$ is even and they are tabulated. The functions $\Theta_{l_1,l_2,l}$ are calculated and stored on a grid; the values at any distance R can be looked up using a spline interpolation.

5.3.1 Fast Fourier-Bessel transform

In order to obtain (5.22) and thus any two-center integrals, we need to calculate efficiently integrals of the form

$$\chi_l(k) = \sqrt{\frac{2}{\pi}}(-i)^l \int_0^\infty r^2 j_l(kr) \chi_l(r) dr. \tag{5.26}$$

The spherical Bessel functions can be written, in general, as

$$j_l(kr) = \frac{P_l^s \sin(kr) + P_l^c \cos(kr)}{(kr)^{l+1}}, \tag{5.27}$$

where $P_l^{s,c}$ are polynomials. By using trigonometric identities, we can write

$$j_l(kr) = \frac{1}{(kr)^{l+1}} \Re \left[P_l(kr) e^{-ikr} \right], \tag{5.28}$$

where $P_l(kr) = P_l^c(kr) + i P_l^s(kr)$ and it obeys the recurrence relation [2]

$$\begin{aligned} &P_0(kr) = i \\ &P_1(kr) = i - x \\ &P_{l+1}(kr) = (2l+1) P_l(kr) - (kr)^2 P_{l-1}(kr). \end{aligned} \tag{5.29}$$

In order to apply the Fast Fourier Transform algorithm we write $P_l(kr) = \sum_i^l C_{li}(kr)^i$ and get the coefficients C_{li} from (5.29):

$$\begin{aligned}\chi_l(k) &= \sqrt{\frac{2}{\pi}}(-i)^l \int_0^\infty \frac{r^2}{(kr)^{l+1}} \Re\left[\sum_i C_{li}(kr)^{l+1} e^{-ikr}\right] \chi_l(r) dr \\ &= \sum_i k^{i-l-1} \Re\left[C_{li} FFT\{r^{1+i-l}\chi_l(r)\}\right],\end{aligned} \tag{5.30}$$

where the FFT operator is a fast discrete Fourier transform, defined as

$$X[k] = \sum_{m=0}^{n-1} x[m]\, e^{-i\frac{2\pi km}{n}} = FFT\{x[m]\}. \tag{5.31}$$

Some technicalities concerning the implementation of this FFT are reported in Appendix A.

5.4 Grid integrals

The matrix elements of the effective potential $V^{\text{eff}} = u_H[\tilde{\rho}] + v_{xc}[\tilde{n}]$ in the Hamiltonian (5.11) are evaluated numerically on the real-space grid.

Because of the localized character of the basis orbitals, matrix elements between basis orbitals which are far apart from each other are exactly zero. In order to take advantage of this sparsity small auxiliary boxes are constructed around each atom, big enough to contain all of the atom's basis functions. Then, with the help of a neighbour list, we can evaluate the effective potential only in the regions where these boxes overlap. In this way one doesn't need to put the localized functions onto the large unit-cell grid.

5.5 Near linear dependence

The Kohn-Sham generalized eigenvalue problem (5.11) is well defined if $\hat{\tilde{H}}$ is hermitian and $\hat{S}$ is positive definite. In this case, in fact, $\hat{S}$ is non-singular and therefore invertible. The eigenvalue problem can then be solved for the eigenvectors C. Linear dependence in the basis set results in a singular overlap matrix $\hat{S}$, thus making the problem ill-defined.

In periodic systems, the basis states are Bloch states, as seen before

$$\Phi_\mu(\mathbf{k}) = \sum_{\mathbf{R}} \Phi_\mu(\mathbf{r} - \mathbf{R}) e^{i\mathbf{k}\cdot\mathbf{R}}, \tag{5.32}$$

where $\mathbf{R}$ is a lattice vector. When we have large overlaps between similar basis functions, as is the case of e.g. crystals, then the basis-set can become nearly linear dependent. Because of the finite numerical precision of

the computation, this leads to a singular overlap matrix within the available accuracy [26]. Due to numerical noise we can even observe negative eigenvalues in some pathological cases.

In other words, this phenomenon occurs when non-orthogonal basis functions on different sites tend to produce large overlaps. This large off-diagonal terms in the overlap matrix $\hat{S}$ can lead to very small eigenvalues, which might be numerically troublesome. As a simple example which shows how the problem might arise, let us consider a simple tight-binding model. For the sake of simplicity let us assume a one-dimensional chain, with only one basis orbital per atom and with nearest-neighbour overlap (hopping) s

$$\epsilon(\mathbf{k}) \sim \frac{2t\cos(ka)}{1+2s\cos(ka)}. \tag{5.33}$$

If we consider the gamma point, for further simplicity, we see that the energy diverges, i.e. the overlap matrix becomes singular in the general case, when $s = -1/2$.

In order to solve the problem, we diagonalize the overlap matrix $\hat{S}$ and check the eigenvalues. If there are eigenvalues smaller than a given threshold, they are removed, together with their correspondent eigenvectors. The Hamiltonian is then diagonalized in this new, smaller, basis where the overlap $\hat{S}$ is diagonal.

5.6 Summary

In this chapter we have derived the expressions for the overlap and Hamiltonian operators in PAW, when a set of atomic-like functions is employed as a basis. In order to set up the Kohn-Sham equation (5.11), we need to construct the overlap operator and the Hamiltonian. The overlap operator itself and all the two-center integrals between projector and basis functions are calculated analytically through the Fourier-Bessel transform. The kinetic matrix elements $\langle\phi_\mu| - \frac{1}{2}\nabla^2|\phi_\nu\rangle$ can also be calculated in the same way, provided that we add an extra $\frac{1}{2}k^2$ factor in (5.24), equivalent to the $-\frac{1}{2}\nabla^2$ operation in the reciprocal space. Since the density is represented on the grid, matrix elements with the effective potential are integrated numerically:

$$\begin{aligned}
\langle\psi_{i\mathbf{k}}|\,\hat{H}\,|\psi_{j\mathbf{k}}\rangle = &\sum_{\mu,\nu} c^*_{\mu i\mathbf{k}} c_{\nu j\mathbf{k}} \sum_{\bar{\mathbf{R}}} \underbrace{\langle\phi_{\mu\mathbf{0}}|\hat{T}|\phi_{\nu\bar{\mathbf{R}}}\rangle}_{two-center} e^{i\mathbf{k}\cdot\bar{\mathbf{R}}} + \\
&+ \sum_{\mu,\nu} c^*_{\mu i\mathbf{k}} c_{\nu j\mathbf{k}} \sum_{\bar{\mathbf{R}}} \underbrace{\langle\phi_{\mu\mathbf{0}}|\hat{V}_{eff}|\phi_{\nu\bar{\mathbf{R}}}\rangle}_{grid-integral} e^{i\mathbf{k}\cdot\bar{\mathbf{R}}} + \\
&+ \sum_{\mu,\nu} c^*_{\mu i\mathbf{k}} c_{\nu j\mathbf{k}} \sum_{a,i_1,i_2} \Delta H^a_{i_1 i_2} \left(\sum_{\mathbf{R}} \underbrace{\langle\phi_{\mu\mathbf{R}}|\tilde{p}^{a,\mathbf{0}}_{i_1}\rangle}_{two-center} e^{i\mathbf{k}\cdot\mathbf{R}} \right) \left(\sum_{\mathbf{R}'} \underbrace{\langle\tilde{p}^{a,\mathbf{0}}_{i_2}|\phi_{\nu\mathbf{R}'}\rangle}_{two-center} e^{i\mathbf{k}\cdot\mathbf{R}'} \right).
\end{aligned} \tag{5.34}$$

Here are a few remarks, which point out the relevant differences with a full real-space grid calculation:

1. There is no need to put the Kohn-Sham wavefunctions on the grid, since the variational parameters are the expansion coefficients of the basis set.

2. The diagonalization of Kohn-Sham generalized eigenvalue problem is done in one step, for the full Hilbert space spanned by the basis functions. In the grid case, one needs to proceed iteratively.

3. Convergence has to be tested against the basis-set quality, and not just against the grid spacing. This can be quite painful and requires some practical experience in generating good basis-sets for a given application.

Chapter 6

Results

I have implemented the expressions derived in Chapter 5 in the GPAW code. In this chapter I present the numerical results and performances of this implementation, which I will call GPAW-LCAO in order to differentiate if from the standard GPAW grid-mode. In order to do so, the GPAW-LCAO scheme is applied to a variety of benchmark calculations against the GPAW grid-mode results.

6.1 Convergence issues

6.1.1 Grid spacing

The main convergence parameter in GPAW is the grid spacing h, i.e. the spacing of the 3D mesh used for the finite-difference method.

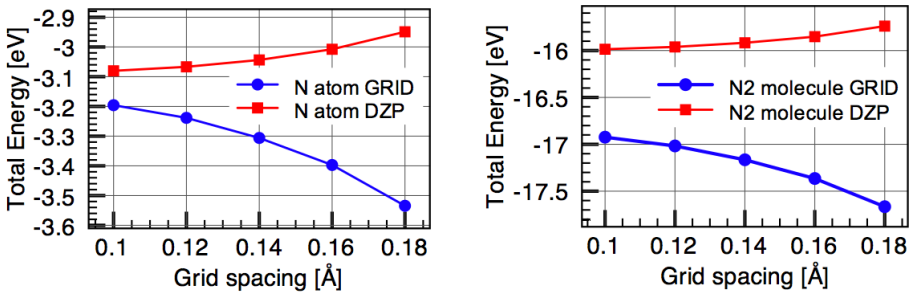

(a) *N atom: energy convergence vs h* **(b)** *N2 molecule: energy convergence vs h*

Figure 6.1: *Convergence of total energy for a DZP basis* $\Delta E = 0.01eV$ *and for the grid.*

As we see from figure (6.1), the convergence of total energy versus the grid-spacing is faster with the LCAO basis than with the full-grid. This is due to the fact that fewer objects are put on the grid in an LCAO calculation. First of all the wavefunction is not present at all, as we only work with the

expansion coefficient of the basis-set. Second, the kinetic-energy matrix elements and the overlaps are calculated analytically. We also notice that the LCAO energy only converges quantitatively towards the grid energy for $h \to 0$

The convergence of total energy may not be important in real applications, but it is useful as a test for the LCAO since the grid result ideally represents the complete basis-set limit. The more physical atomization energy is showed in (6.2) As we see, energy differences converge faster than

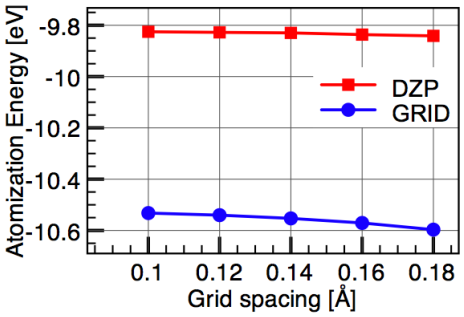

Figure 6.2: *Convergence of atomization energies for a DZP basis* $\Delta E = 0.01eV$ *and for the grid.*

total energies, due to error cancellations. Notice that the basis-set results depend very weakly on the grid-spacing.

6.1.2 Basis size/quality

Unlike plane wave basis sets or real-space grids, there is no such thing as a single parameter controlling the convergence with respect to the size of the basis set. In fact, adding more basis orbitals does not automatically ensure better accuracy. This is why we can talk about "quality" of a basis-set, pointing out that the number of basis functions is not the only parameter with a role in the resulting accuracy. Nevertheless, the split valence method we employ shows rather systematic improvements in the accuracy with increasing size of the basis, see Fig. (6.3).

Besides the number of basis functions, their cut-off radii play an important role. For each particular application one has to find a trade off between short-ranged basis functions, which improve efficiency, and longer ranged functions, which improve accuracy. This is for instance especially important for isolated atoms, for which a large cut-off is usually needed in order to approach the grid result. See Fig. (6.4).

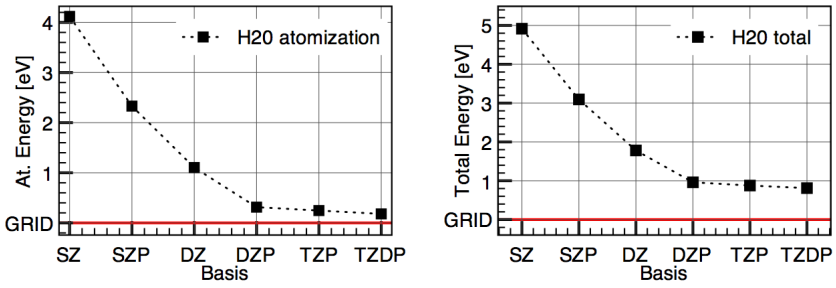

(a) *H_2O atomization energy* **(b)** *H_2O total energy*

Figure 6.3: *Convergence of total (6.3a) and atomization (6.3b) energies for different basis sets with respect to the grid.*

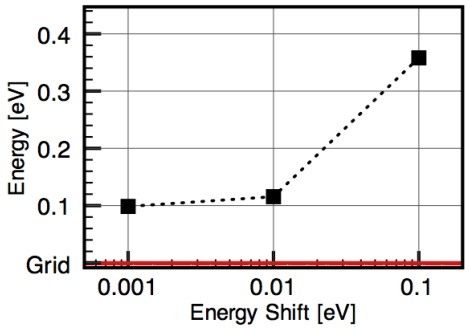

Figure 6.4: *Total energy of N atom, relative to grid.*

6.2 Small molecules

6.2.1 Atomization energies

In order to assess the results for small molecules, the atomization energies for the G2-1 data-set ([11]) are shown in figure (6.5). What I am plotting is the basis set atomization energy minus the grid atomization energy, defined as

$$\Delta E^{at} = E^{basis}(\text{mol}) - \sum_{atoms} E^{basis}(\text{at}) - \left(E^{grid}(\text{mol}) - \sum_{atoms} E^{grid}(\text{at}) \right) \tag{6.1}$$

For the full plot, showing also all the DZ points falling out of the axis range and for more data, see Appendix C.

Note the qualitative difference from 6.5a and 6.5b. In the latter the energy shift is not small enough to converge the energy for the isolated atoms. This is the reason why we observe points both above and below the grid results. Once the isolated atom's energy is converged, within a given

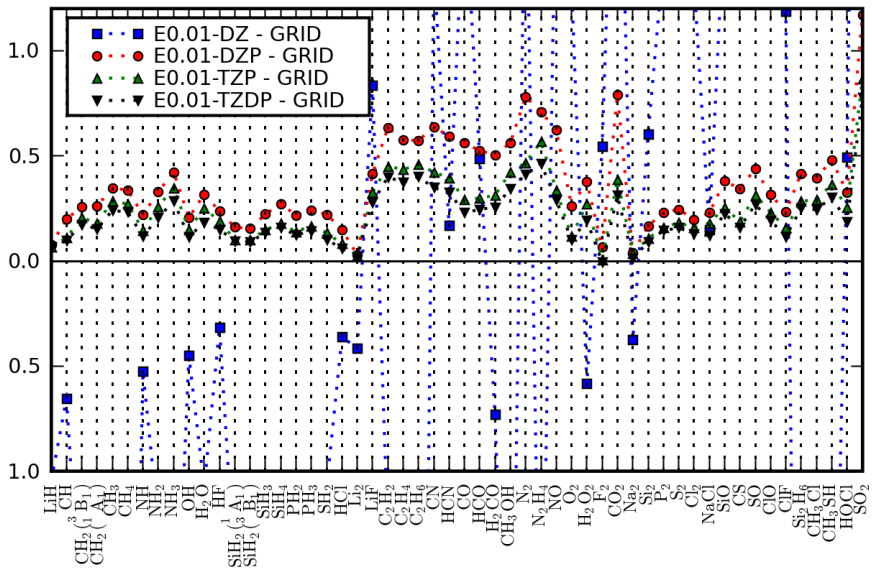

(a) $\Delta E = 0.01eV$

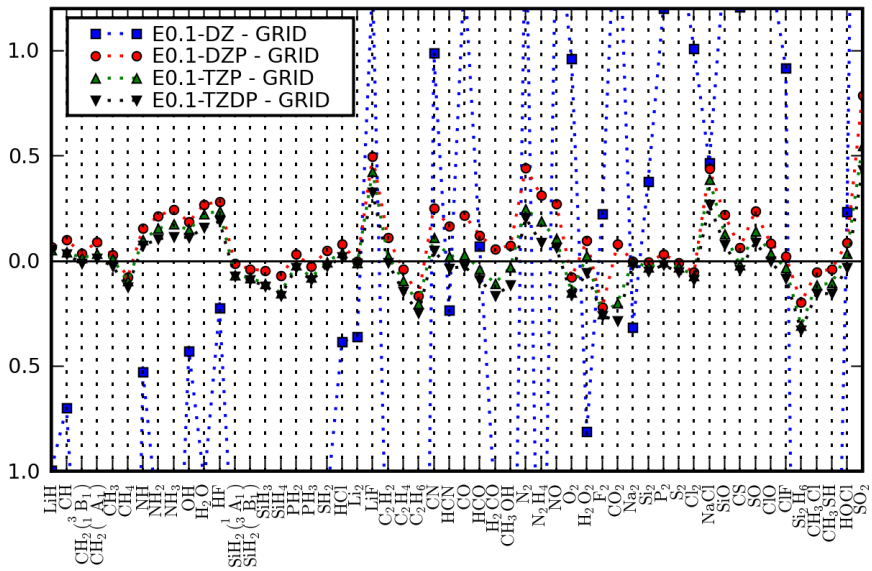

(b) $\Delta E = 0.1eV$

Figure 6.5: *Atomization energies of the G2-1 dataset of small molecules for different basis sets and for two different energy shifts. Energies are relative to the grid values.*

basis-set, all the points move consistently above the zero-line, and converge to it with increasing basis quality, from above as E^{basis}(mol) becomes lower.

The Mean Absolute Errors (MAE) corresponding to Fig.(6.5a) are shown in Table 6.1.

	MAE [eV]	MAE % [eV]
DZ	1.71	20.4
DZP	0.36	4.45
TZP	0.25	3.02
TZDP	0.20	2.44

Table 6.1: *Mean Absolute Errors to the grid for the atomization energies of the G2-1 database for* $\Delta E = 0.01eV$

The same trend is observed for atomization energies calculated with the SIESTA code and compared to plane-wave (PW) calculations performed using the same pseudopotential. For example SIESTA underestimates the binding energy of water with respect to PW's by $0.37eV$ with a DZP basis [19]. I have obtained a difference from the grid of $0.32eV$ with a DZP basis.

6.2.2 Bond lengths

Figure (6.6) shows two examples of total energy curves for molecules as a function of the inter-atomic distance. Different lines refer to different basis sets, as indicated in the legends.

Notice that the shape of the DZP curves, and hence their minima, is very close to the grid result. As I have verified for several other molecules, even smaller basis sets are often able to produce very good estimates of the grid results.

It is also worth noting that the curves calculated with an energy shift of $0.1eV$ have the same shape as the ones with $0.01eV$. They are usually translated in energy by less than $0.1eV$ with respect to each other, but reproduce the same equilibrium value. The more computationally efficient[1] $0.1eV$ energy-shift can then be used without compromising the accuracy of the result.

6.2.3 Computational details

The atomization energy is obtained as the difference between the total energy of the molecule and the sum of the energies of the isolated constituent atoms

$$E^{cohesive} = E^{solid}(a_0) - \sum_i E_i^{atom} \tag{6.2}$$

where i runs over the number of atoms in the unit cell. The atoms are calculated in their spin-polarized ground state. The structure of the molecules

[1] Remember that basis orbitals generated with larger energy shifts are more localized, and high efficiency requires the orbitals to be as localized as possible.

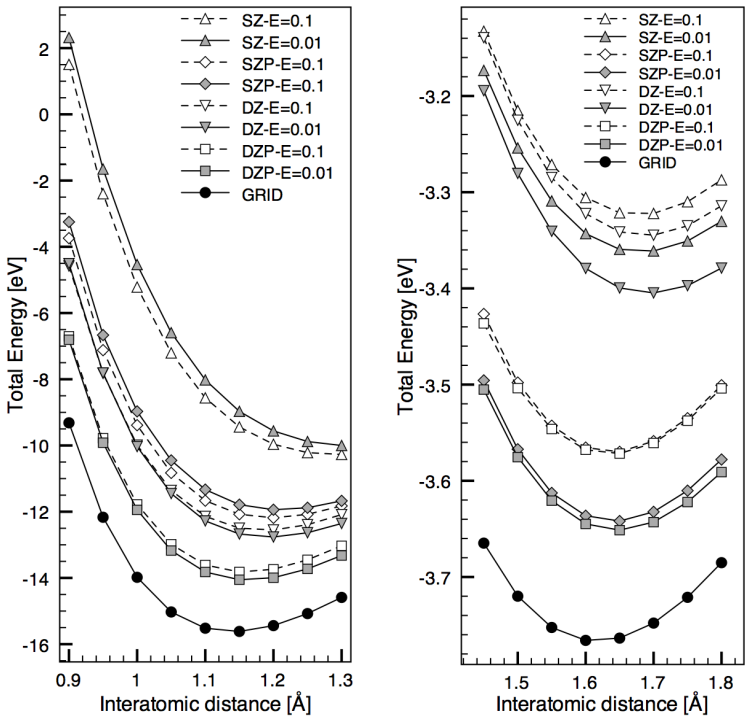

Figure 6.6: *Equilibrium bond lengths for a CO molecule (left panel) and a LiH molecule (right panel). Full lines corresponds to an energy shift of* $0.01eV$ *whereas dashed lines to* $0.1eV$.

has been fixed to the relaxed geometry from a grid calculation. The grid spacing was set to $h = 0.18\mathring{A}$ and the size of the unit-cell to $(12 \times 13 \times 14)\mathring{A}$.

The bond lengths are obtained by performing total energy calculations with different distances between the atoms, selected in the range $\pm 5\%$ from some accurate PBE result.

6.3 Solids

6.3.1 Theoretical equilibrium properties

The equilibrium bulk properties have been calculated for several crystals. Different kinds of electronic behavior are considered in order to obtain a good overview: simple metals (Li, Na, Al), semiconductors (AlP, Si, SiC), ionic solids (NaCl, LiF, MgO) as well as transition metals (Ag, Cu). A summary table is shown in table 6.2. All the calculations were performed with the solids in their lowest energy crystal structure and spin-paired, i.e. non magnetic ground states.

	a(Å)				
	SZP	DZ	DZP	TZP	GRID
LiF	4.09	4.11	4.12	4.10	4.13
Ag	4.22	4.18	4.19	4.20	4.19
C	3.59	3.58	3.58	3.58	3.58
Na	4.22	4.32	4.30	4.27	4.20
MgO	4.30	4.32	4.31	4.28	4.28
Al	4.07	4.09	4.07	4.06	4.04
NaCl	5.68	5.70	5.69	5.69	5.71
Li	3.47	3.77	3.44	3.45	3.45
SiC	4.41	4.48	4.40	4.40	4.41
Si	5.51	5.58	5.50	5.49	5.48
AlP	5.54	5.58	5.53	5.53	5.52
Cu	3.65	3.66	3.66	3.66	3.66
MAE	0.023	0.073	0.022	0.016	
MAE %	0.51	1.79	0.50	0.37	
	E_c(eV)				
	SZP	DZ	DZP	TZP	GRID
LiF	-4.10	-4.18	-4.24	-4.27	-4.21
Ag	-2.22	-2.32	-2.38	-2.43	-2.56
C	-7.29	-7.49	-7.67	-7.69	-7.72
Na	-0.93	-1.01	-1.01	-1.02	-1.11
MgO	-3.66	-4.79	-4.79	-4.86	-4.95
Al	-3.33	-3.20	-3.36	-3.37	-3.44
NaCl	-2.92	-3.10	-3.09	-3.10	-3.14
Li	-1.54	-1.25	-1.58	-1.58	-1.62
SiC	-6.02	-5.74	-6.20	-6.22	-6.52
Si	-4.28	-4.09	-4.48	-4.50	-4.56
AlP	-3.84	-3.68	-3.98	-3.98	-4.11
MAE	0.346	0.281	0.111	0.095	
MAE %	9.02	8.10	3.35	2.88	
	B(GPa)				
	SZP	DZ	DZP	TZP	GRID
LiF	83.5	74.9	64.5	73.1	65.8
Ag	80.1	84.1	81.6	86.2	91.1
C	414.8	441.3	433.7	433.9	434.3
Na	7.9	7.9	7.0	7.0	8.0
MgO	157.9	166.8	156.9	144.0	143.5
Al	76.2	91.5	69.4	76.2	78.3
NaCl	28.7	27.6	25.6	25.3	23.4
Li	16.4	7.0	16.5	14.8	14.1
SiC	207.8	205.9	216.1	210.2	195.9
Si	83.5	72.0	85.4	87.5	88.8
AlP	78.3	81.5	80.3	81.4	80.3
Cu	140.4	164.3	133.6	131.5	119.7
MAE	8.327	9.000	5.718	3.227	
MAE %	10.08	13.75	7.85	5.03	

Table 6.2: *Lattice constants a, cohesive energies E_c and bulk moduli for selected solids. Errors are relative to the converged grid results. $\Delta E = 0.01eV$ for all the basis sets.*

The overall agreement with the real-space grid is very good, that is to say about 0.5% mean absolute error in the computation of lattice constants, 3% in cohesive energies and 5-8 % for bulk moduli. Notice than in many cases a remarkably good results can be obtained with a small SZP basis, especially for a and B.

As a benchmark against other available methods, I report some results for the SIESTA code in table 6.3. Note that these results were obtained with accurately optimized basis-sets and with the LDA approximation for the exchange and correlation functional. The deviation of the basis results from the plane-wave results compares well with the deviations of our basis results from the grid.

	a(Å)		**E_c(eV)**		**B(GPa)**	
	DZP	PW	DZP	PW	DZP	PW
C	3.53	3.54	8.90	8.81	466	453
Si	5.38	5.40	5.37	5.31	96	97
Na	3.95	3.98	1.22	1.22	8.8	9.2
MgO	4.10	4.11	11.90	11.87	168	167

Table 6.3: *Siesta (DZP) results compared to plane wave calculations (PW) using the same pseudopotential. Adapted from [19].*

Details on how the theoretical equilibrium properties have been calculated are reported in the following section.

6.3.2 Band structures

Another benchmark calculation for solid-state crystalline systems is the band diagram. Figure (6.7) and (6.8) shows the calculated band structure respectively for bulk Silicon and for a 2D graphene sheet. The band structures are calculated along the $\Gamma - X$ direction of the Brillouin zone. Excellent agreement with the grid result is achieved.

6.3.3 Computational details

In order to obtain the equilibrium properties of the solids, the total energy per unit cell has been calculated for 7 different lattice distances in the range $\pm 2\%$ from some accurate PAW-PBE calculation.

The minimum of the total energy curve versus the lattice distance gives the equilibrium lattice constant. This is calculated by finding the minimum of a second order polynomial fitted to the data

The cohesive energy is obtained as the difference between the total energy of the solid calculated at the theoretical equilibrium a_0 and the sum of the

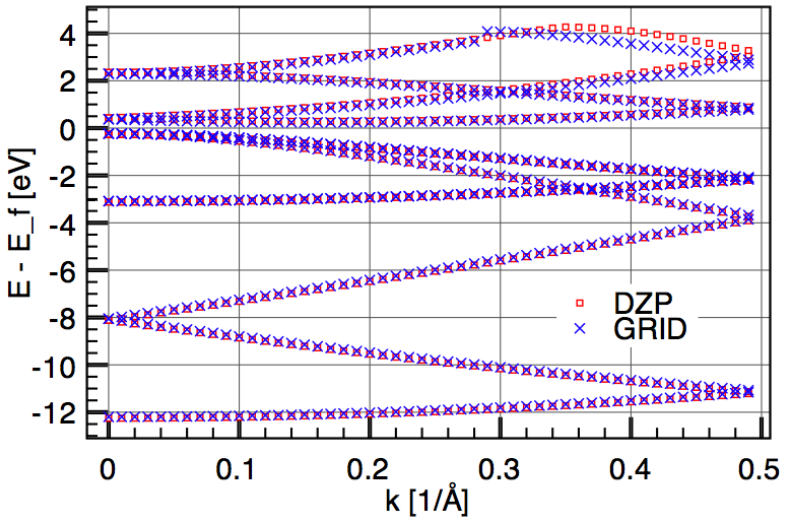

Figure 6.7: *Band structure of bulk Si. Basis set points are represented by red squares and grid points by blue crosses.*

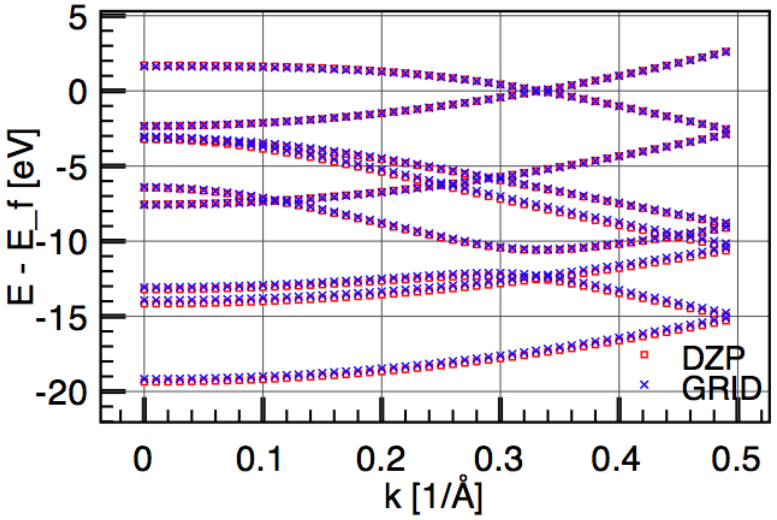

Figure 6.8: *Band structure of graphene. Basis set points are represented by red squares and grid points by blue crosses.*

energies of the isolated constituent atoms

$$E^{cohesive} = E^{solid}(a_0) - \sum_i E_i^{atom}, \tag{6.3}$$

where i runs over the number of atoms in the unit cell. The atoms are calculated in their spin-polarized ground states.

The bulk modulus is calculated as

$$B = V \frac{\partial^2 E}{\partial V^2}\Big|_{V=V_0}, \tag{6.4}$$

where V is the volume of the unit cell and V_0 is the theoretical equilibrium volume. This expression is evaluated by fitting the data to a third order polynomial.

The band structures are obtained by calculating the density with a standard self-consistent Kohn-Sham calculation. The energies at different k-points are then evaluated through the non self-consistent Harris functional, i.e. keeping the density fixed.

6.4 NEGF and Electron Transport

Non-equilibrium Green's functions can be combined with DFT to investigate electron transport in the so called NEGF-DFT scheme [8]. The structure and the electronic properties are calculated with DFT, and the Kohn-Sham Hamiltonian in a localized representation is used to calculate the Green's functions of the system. They are in turn used to calculate the Landauer-Buttiker transmission function. The zero-temperature, linear response conductance of non-interacting electrons through a scattering central (C) region between to leads (L,R) is given by

$$G(\varepsilon) = G_0 T(\varepsilon_F), \tag{6.5}$$

where $G_0 = 2e^2/h$ is the conductance quantum and $T(\varepsilon)$ is the transmission function, given by

$$T(\varepsilon_F) = Tr[G^r(\varepsilon)\Gamma_L(\varepsilon)G^a(\varepsilon)\Gamma_R(\varepsilon)], \tag{6.6}$$

where $\Gamma_{L/R}$ are related to the self-energies $\Sigma_{L/R}$ of the leads by

$$\Gamma_{L/R} = i(\Sigma_{L/R} - \Sigma^\dagger_{L/R}). \tag{6.7}$$

In order to evaluate these expressions, the Kohn-Sham Hamiltonian and overlap matrix needs to be expressed in a localized basis.

Figure 6.9 shows the remarkably good agreement between the transmission function calculated with SIESTA (dotted line) and with GPAW-LCAO (full line) for an infinite aluminum mono-atomic wire with atomic hydrogen adsorbed.

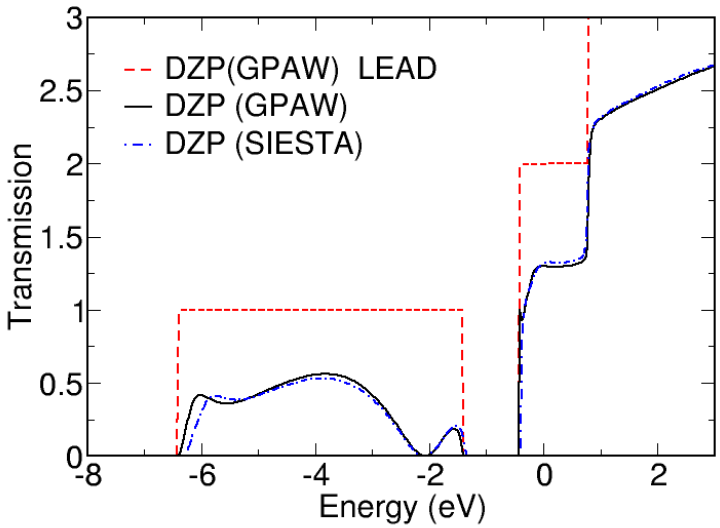

Figure 6.9: *Transmission function for Al mono-atomic wire with adsorbed H. The red dashed line is the transmission function for the infinite bare wire.*

Chapter 7

Conclusion and Outlook

The benchmark results presented in Chapter 6 demonstrate good agreement between the PAW results one can obtain with efficient basis sets and with the grid. Since nothing comes for free, one has to put some efforts in generating good basis sets for a given application. Nevertheless the approach we employ seems to provide a quite systematic method to improve the quality of a given basis.

It is worth noting that the errors with respect to a grid calculation lie well within the accuracy of the PBE functional. As showed in [17], for example, the mean absolute error of the PBE functional for cohesive energies of solids is $0.16eV$. Our mean absolute error to the grid is $0.11eV$ with a DZP basis.

The work presented in this thesis is the first implementation of a localized basis in the PAW formalism, and hence it needs further investigation in order to fully understand strengths and limits.

Future plans include testing the basis results for large realistic systems. In order to do this, it will be necessary to implement a correction scheme for the basis set superposition error. The Counterpoise method could be employed by introducing "ghost" atoms, i.e. special PAW setups only containing basis functions but no electrons and nuclear charge.

Some work could also be done in order to obtain optimized high-quality basis sets. A method to variationally optimize[1] a given basis should be developed in order to both simplify the generation procedure and to go beyond the restrictive energy-shift criterion for fixing the cut off radii of the basis orbitals.

The parallelization, already implemented in a preliminary form, needs to be optimized in order to fully test the capabilities of handling very large and complex systems.

[1] i.e. optimize the parameters which enter the expression for a given basis function by minimizing the total energy of some reference system.

Appendix A

Fast Fourier Transform

The discrete Python FFT is defined as

$$X\left[k\right] = \sum_{m=0}^{n-1} x\left[m\right] e^{-i\frac{2\pi km}{n}} = FFT\{x\left[m\right]\}. \tag{A.1}$$

where $x\left[m\right]$ is an input array, in our case some localized functions, and $X\left[k\right]$ is the output array in the reciprocal variable k.

The FFT algorithm is most efficient when the number of grid points of the input array is $N = 2^x$, where x is a even integer. Most modern implementations are less restrictive and allow for different lengths as well. In the optimal case the number of operations scale as $O(N \log_2 N)$, as is shown in (A.1).

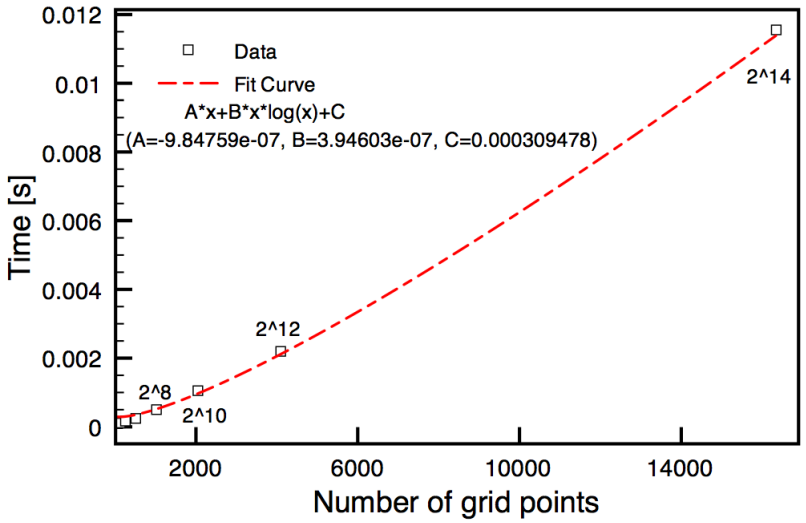

Figure A.1: *Fit of FFT time as a function of the number of grid points showing the typical $N \log N$ scaling.*

In order to increase the spectral resolution, i.e. the resolution of $X[k]$, we can zero-pad the input array. In this way we both increase the resolution and the efficiency, as we can select the length of the padding so that we get $N = 2^x$ with an even x. I found $N = 2^{12}$ a reasonable compromise for the number of grid points. This is also in agreement with the rule of thumb which suggests a zero-padding to 4 times the input's length.

A straightforward, though not optimal, way to select a reasonable N is to look at the total energy of a simple system as a function of N and pick a value that produces a well converged total energy.

Appendix B

Implementation details

Figure (B.1) shows the general structure of the GPAW code. The grey rectangles represent Python classes. In red are the major new classes I have

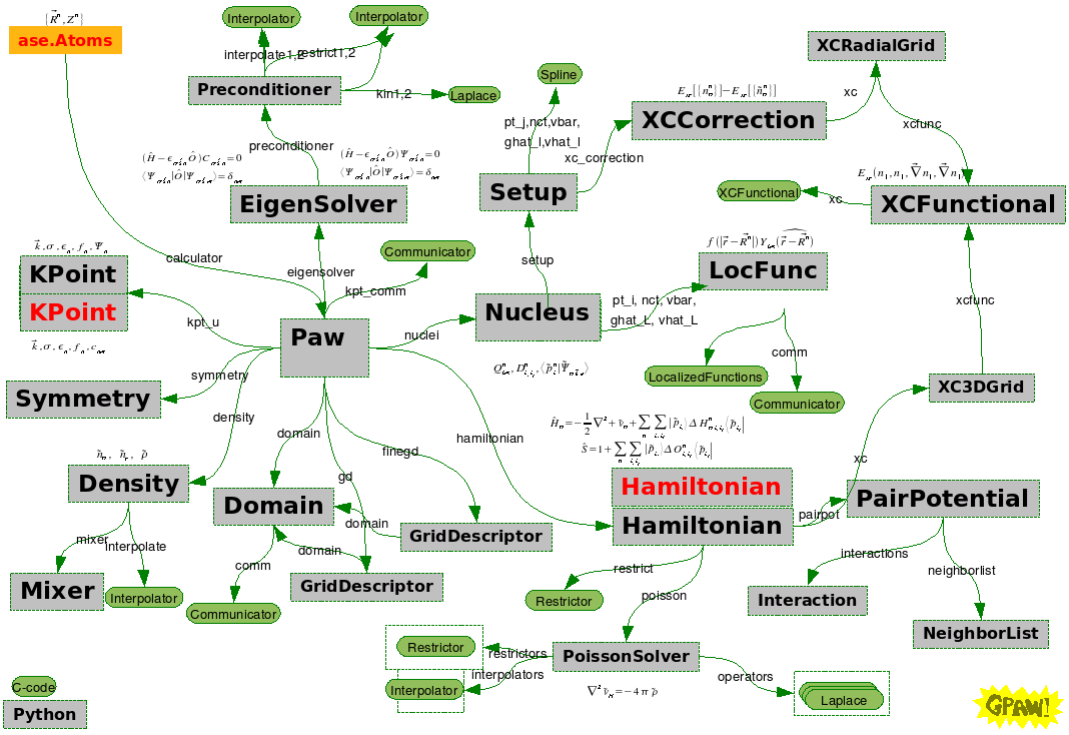

Figure B.1: *The "under-the-pillow" GPAW big picture.*

implemented in order to handle a basis-set calculation.

The `Hamiltonian` class sets up the hamiltonian by adding together the effective Kohn-Sham potential, which is calculated on the grid, and the kinetic energy, which is calculated analytically by a special `TwoCenterIntegrals`

class. The latter class also calculates the overlap matrix which is used for solving the generalized Kohn-Sham equations.

The `K-point` class no longer contains the Kohn-Sham wavefunctions, but rather the expansion coefficients of the basis set. These are obtained as solution of the Kohn-Sham equation, performed by the `Eigensolver` class.

The `Eigensolver` class includes a new eigensolver which diagonalizes the Kohn-Sham hamiltonian in one go, within the basis-set representation. It also takes care of removing possible linear dependence which would cause the overlap matrix to become singular and thus the diagonalization to fail.

Appendix C

Scalar relativistic Schrödinger equation

In GPAW, projector functions and partial waves, i.e. the so-called "PAW-setups", are generated taking into account scalar-relativistic effects. In order for the basis functions to be consistent with the corresponding setups, we generates the single-zeta functions from a scalar-relativistic all-electron equation

$$-\frac{d^2u_{nl}}{dr^2} - \frac{\alpha^2}{2M}\frac{dV^{\text{eff}}}{dr}\left(\frac{du_{nl}}{dr} - \frac{u_{nl}}{r}\right) + \left[\frac{l(l+1)}{r^2} + 2M(V^{\text{eff}} - \varepsilon_{nl})\right]u_{nl} = 0 \tag{C.1}$$

where M is the relativistic electron mass

$$M = 1 - \frac{\alpha^2}{2}(V^{\text{eff}} - \varepsilon_{nl}), \tag{C.2}$$

$u_{nl}(r)$ is r times the radial function and $\alpha \simeq 1/137$ is the fine-structure constant. Note that in the case of $\alpha \to 0$ one recovers the non-relativistic limit.

Note that equation (C.1) contains the so called "scalar-relativistic" corrections. This means that the spin-orbit coupling which appears in the Dirac equation is dropped.

For most elements across the periodic table relativistic corrections for the valence states are totally negligible as far as the ground state energetics is concerned. For 4-d and 5-d metals, on the other hand, they can be quite important in some cases. As an example, Fig C.1 shows the Single-Zeta basis functions for Pt, generated from a non relativistic calculation (full lines) and from a relativistic calculation (dashed lines)

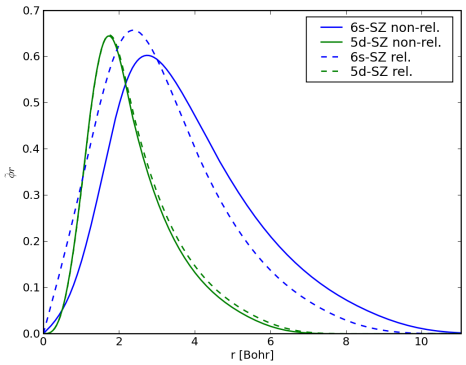

Figure C.1: *Single zeta basis orbitals for Pt. Non relativistic states are full lines, relativistic states are dashed lines.*

Bibliography

[1] The GPAW code is freely available at https://wiki.fysik.dtu.dk/gpaw.

[2] M. Abramowitz and I. A. Stegun. *Handbook of Mathematical Functions*. New York: Dover, 1964.

[3] Emilio Artacho, E Anglada, O Diguez, J D Gale, A Garca, J Junquera, R M Martin, P Ordejn, J M Pruneda, D Snchez-Portal, and J M Soler. The siesta method; developments and applicability. *Journal of Physics: Condensed Matter*, 20(6):064208, 2008.

[4] A. D. Becke. Density-functional exchange-energy approximation with correct asymptotic behavior. *Physical Review A*, 38:3098–3100, 1988.

[5] P. E. Blöchl. Projector augmented-wave method. *Physical Review B*, 50(23):17953–17979, 1994.

[6] P.E. Blöchl. First-principles calculations of defects in oxygen-deficient silica exposed to hydrogen. *Physical Review B (Condensed Matter)*, 62(10):6158–79, 2000.

[7] S.F. Boys and F. Bernardi. The calculation of small molecular interactions by the differences of separate total energies. some procedures with reduced errors. *Molecular Physics*, 19(4):553–66, 1970.

[8] Brandbyge, M., Mozos, J.-L., Ordejon, P., Taylor, J., and K. Stokbro. Density-functional method for nonequilibrium electron transport. *Physical Review B*, 65(16):165401/1–17, 2002.

[9] Achi Brandt. Multi-level adaptive solutions to boundary-value problems. *Mathematics of Computation*, 31(138):333–390, 1977.

[10] K. Burke, J. P. Perdew, and M. Ernzerhoff. Why semilocal functionals work: Accuracy of the on-top pair density and importance of system averaging. *Journal of Chemical Physics*, 109:3760–3771, 1998.

[11] L.A. Curtiss, Krishnan Raghavachari, P.C. Redfern, and J.A. Pople. Assessment of gaussian-2 and density functional theories for the computation of enthalpies of formation. *Journal of Chemical Physics*, 106(3):1063–79, 1997.

[12] D. Sanchez-Portal E. Artacho, A. Garcia P. Ordejon, and J.M. Soler. Linear-scaling ab-initio calculations for large and complex systems. *Physica Status Solidi B*, 215(1):809–17, 1999.

[13] E. Fermi. Statistical method of investigating electrons in atoms. *Zeitschrift für Physik*, 48:73–79, 1928.

[14] B. Hammer, L. B. Hansen, and J. K. Nørskov. Improved adsorption energetics within density-functional theory using revised Perdew-Burke-Ernzerhof functionals. *Physical Review B*, 59:7413–7421, 1999.

[15] P. Hohenberg and W. Kohn. Inhomogeneous electron gas. *Physical Review*, 136:B864–B871, 1964.

[16] N.A.W. Holzwarth, A.R. Tackett, and G.E. Matthews. A projector augmented wave (paw) code for electronic structure calculations. i. atompaw for generating atom-centered functions. *Computer Physics Communications*, 135(3):329–47, 2001.

[17] L. B Hansen J. J. Mortensen and K. W. Jacobsen. Real-space grid implementation of the projector augmented wave method. *Physical Review B*, 71:035109, 2005.

[18] E Artacho José M Soler, Alberto García Julian D Gale, Pablo Ordejn Javier Junquera, and Daniekl Snchez-Portal. The SIESTA method for ab initio order-N materials simulation. *Journal of Physics: Condensed Matter*, 14:2745–2779, 2002.

[19] J. Junquera, O. Paz, D. Sanchez-Portal, and E. Artacho. Numerical atomic orbitals for linear-scaling calculations. *Physical Review B (Condensed Matter and Materials Physics)*, 64(23):235111/1–9, 2001.

[20] K. Koepernik and H. Eschrig. Full-potential nonorthogonal local-orbital minimum-basis band-structure scheme. *Physical Review B*, 59(3):1743–57, 1999.

[21] W. Kohn. Nobel Lecture: Electronic structure of matter—wave functions and density functionals. *Reviews of Modern Physics*, 71:1253–1266, 1999.

[22] W. Kohn and L. J. Sham. Self-consistent equations including exchange and correlation effects. *Physical Review*, 140:A1133–A1138, 1965.

[23] G. Kresse and D. Joubert. From ultrasoft pseudopotentials to the projector augmented-wave method. *Physical Review B*, 59:1758–1775, 1999.

[24] C. Lee, W. Yang, and R. G. Parr. Development of the Colle-Salvetti correlation-energy formula into a functional of the electronic density. *Physical Review B*, 37:785–789, 1988.

[25] Yi Liu, D.A. Yarne, and M.E. Tuckerman. Ab initio molecular dynamics calculations with simple, localized, orthonormal real-space basis sets. *Physical Review B (Condensed Matter and Materials Physics)*, 68(12):125110–1–8, 2003.

[26] P.O. Lowdin. Band theory, valence bond, and tight-binding calculations. *Journal of Applied Physics*, 33:251–280, 1962.

[27] Journal of Chemical Physics. An all-electron numerical method for solving the local density functional for polyatomic molecules. *Journal of Chemical Physics*, 92(1):508–17, 1990.

[28] C. J. Först P. E. Blöchl and J. Schimpl. Projector augmented wave method: ab-initio molecular dynamics with full wave functions. *Bulletin of Materials Science*, 26:33–41, 2003.

[29] J. P. Perdew and Y. Wang. Accurate and simple analytic representation of the electron-gas correlation energy. *Physical Review B*, 45:13244–13249, 1992.

[30] J. P. Perdew and A. Zunger. Self-interaction correction to density-functional approximations to many-electron systems. *Physical Review B*, 23:5048–5079, 1981.

[31] H.M. Petrilli, P.E. Blöchl, P. Blaha, and K. Schwarz. Electric-field-gradient calculations using the projector augmented wave method. *Physical Review B (Condensed Matter)*, 57(23):14690–7, 1998.

[32] C.J. Pickard and F. Mauri. All-electron magnetic response with pseudopotentials: Nmr chemical shifts. *Physical Review B (Condensed Matter and Materials Physics)*, 63(24):245101/1–13, 2001.

[33] Daniel Sanchez-Portal, Emilio Artacho, and Jose M. Soler. Analysis of atomic orbital basis sets from the projection of plane-wave results. *Journal of Physics Condensed Matter*, 8(21):3859–3880, 1996.

[34] O.F. Sankey and D.J. Niklewski. Ab initio multicenter tight-binding model for molecular-dynamics simulations and other applications in covalent systems. *Physical Review B (Condensed Matter)*, 40(6):3979–95, 1989.

[35] Daniel Snchez-Portal, Emilio Artacho, Jos I. Pascual, Julio Gmez-Herrero, Richard M. Martin, and Jos M. Soler. First principles study of the adsorption of c60 on si(1 1 1). *Surface Science*, 482-485(Part 1):39–43, 2001.

[36] L. H. Thomas. The calculation of atomic fields. *Proceedings of the Cambridge Philosophical Society*, 23:542–548, 1927.

[37] Y. Zhang and W. Yang. Comment on 'Generalized gradient approximation made simple'. *Physical Review Letters*, 80:890, 1998.